



**IAEA**

International Atomic Energy Agency

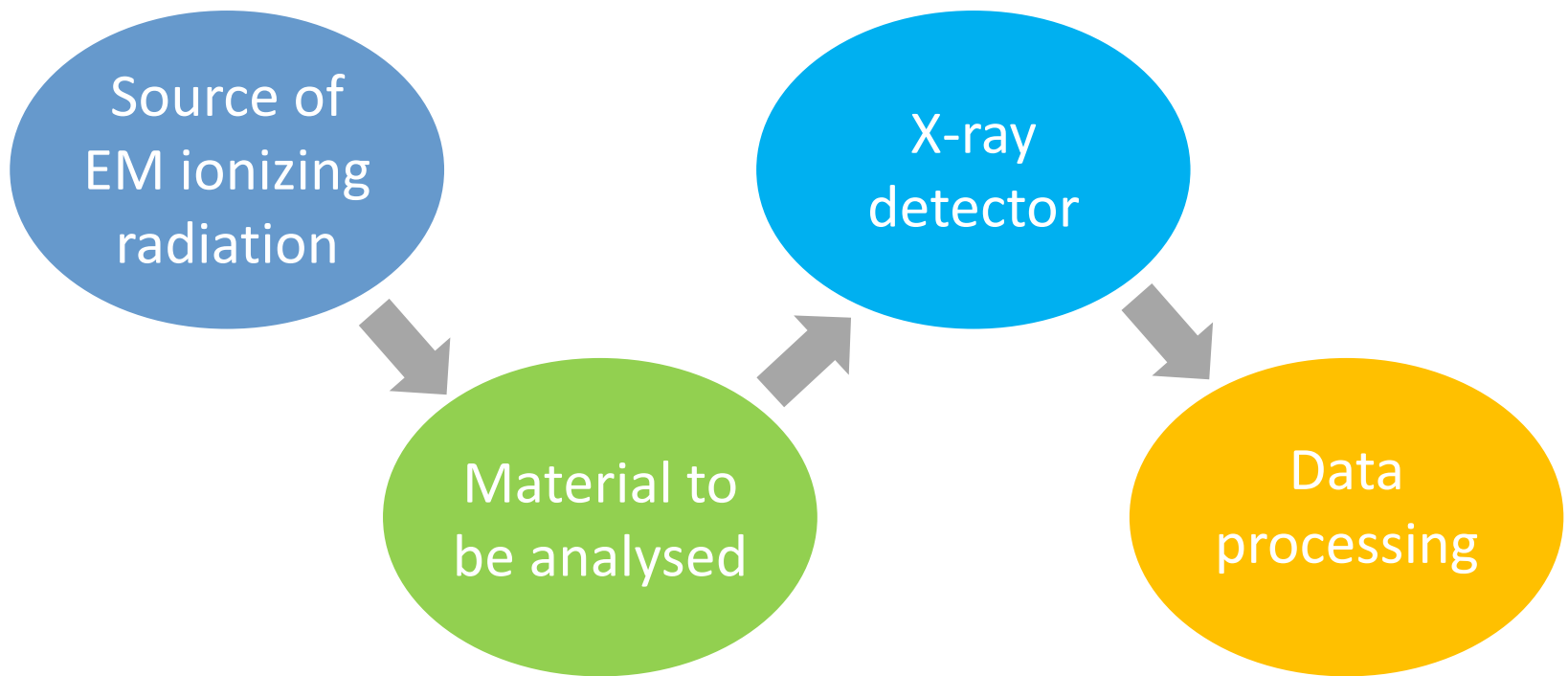
# XRF techniques for materials and life sciences

*Alessandro Migliori*

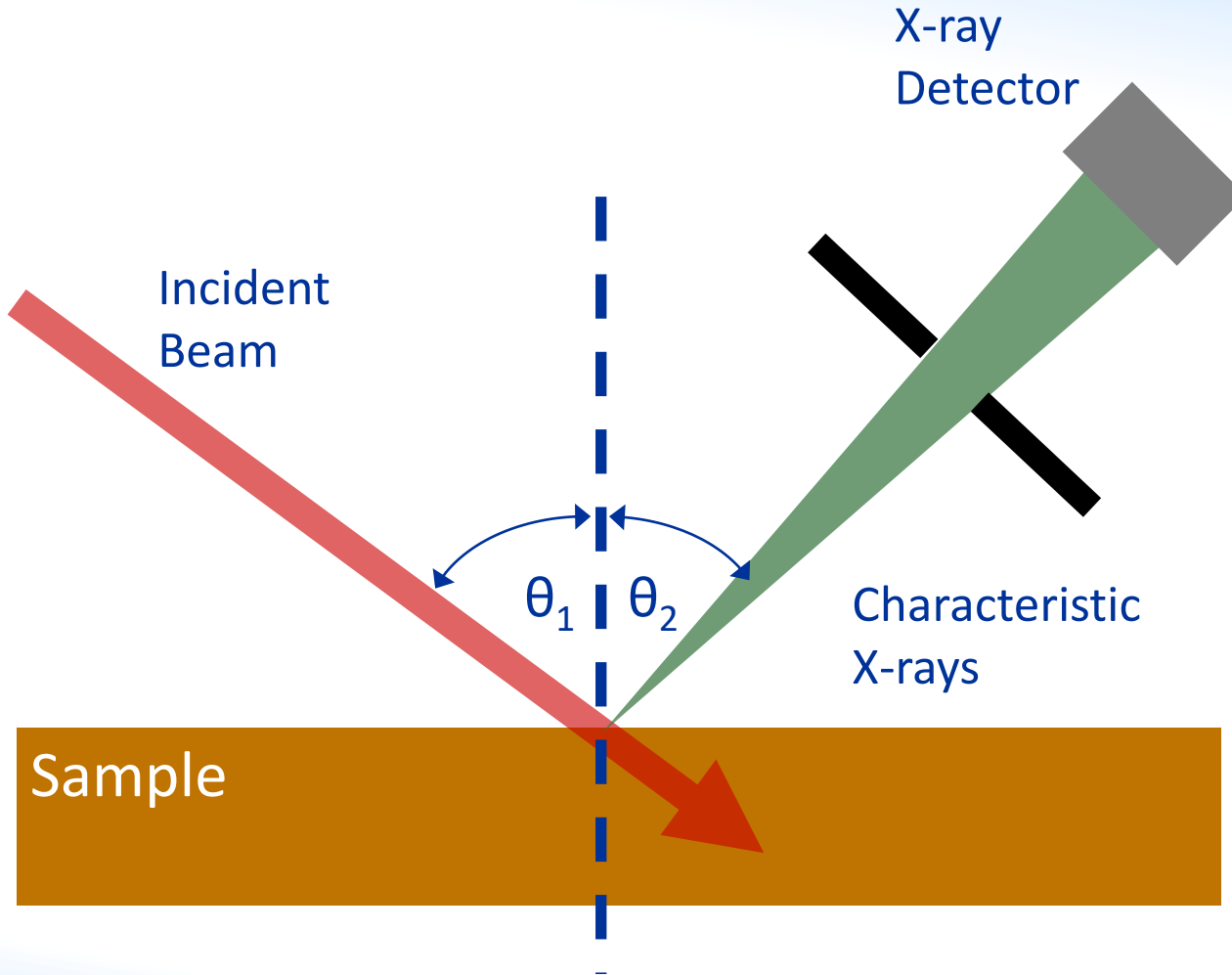
*Nuclear Science and Instrumentation Laboratory*

*International Atomic Energy Agency*

# □ Elements in XRF



# Conventional XRF



# ☐ Sources of ionizing radiation

- Electrons (SEM)
- Charged particles (accelerators)
- Radioisotopes ( $\alpha$ ,  $\gamma$ , **X-rays**)
- **X-ray Tubes**
- **Synchrotron radiation**

# ☐ Interaction of X-rays with matter

X-rays can interact with the atoms of the material in two different ways:

- **Photoelectric effect**: Primary X-ray radiation can ionise atoms of the material. The X-ray is absorbed in this process
- **Scattering**:
  - ✓ **Elastic/Coherent scattering (Rayleigh)**: no energy loss after collision with electrons. The Rayleigh effect is present when electrons are strongly bound (inner atomic electrons)
  - ✓ **Inelastic/Incoherent scattering (Compton)**: energy loss after collision with electrons. The Compton effect is present when electrons are loosely bound (outer, less bound electrons)

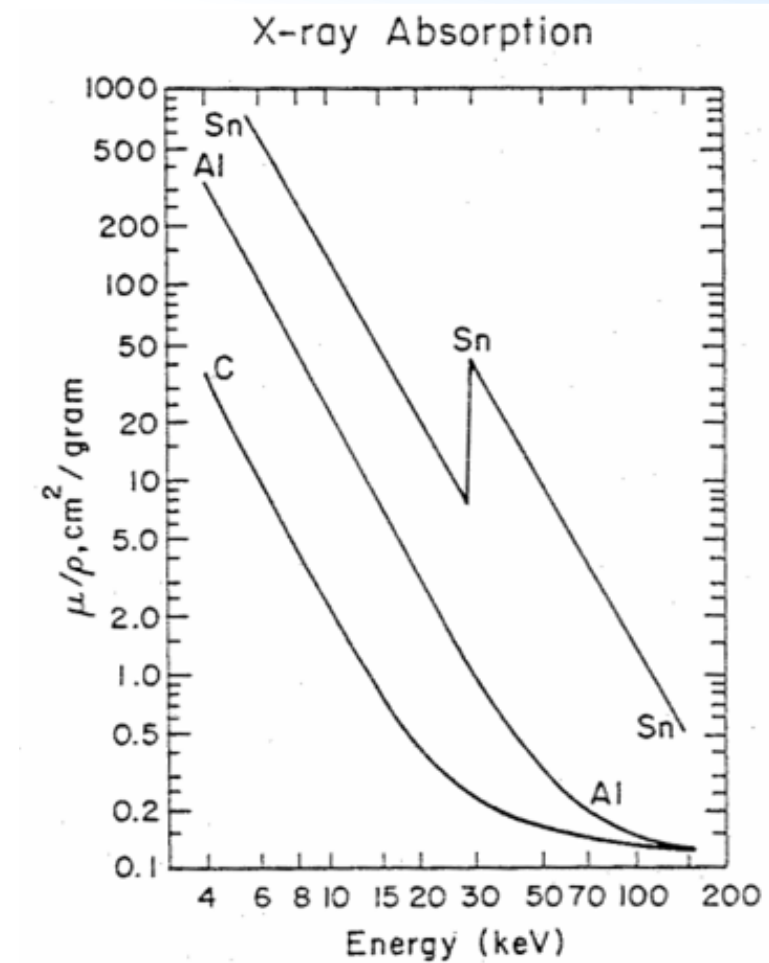
# ☐ Photoelectric effect

**Photoelectric effect:** Primary X-ray radiation can ionise atoms of the material to be analysed

Cross section of the PE depends strongly on  $Z$  of the material and on the energy of the primary X-ray

$$\sigma_{Ph} \propto \frac{Z^n}{E_X^{3.5}} \quad n = 3 \div 4$$

To maximize the ionization probability, the energy of the primary X-ray should be higher than the binding energy but as close as possible to it



# X-Ray Fluorescence

Incident photon  
Energy  $E_0$   
should be adequate  
to ionize the atomic  
bound electrons  
→  $E_0 \geq$  inner shell  
binding energy

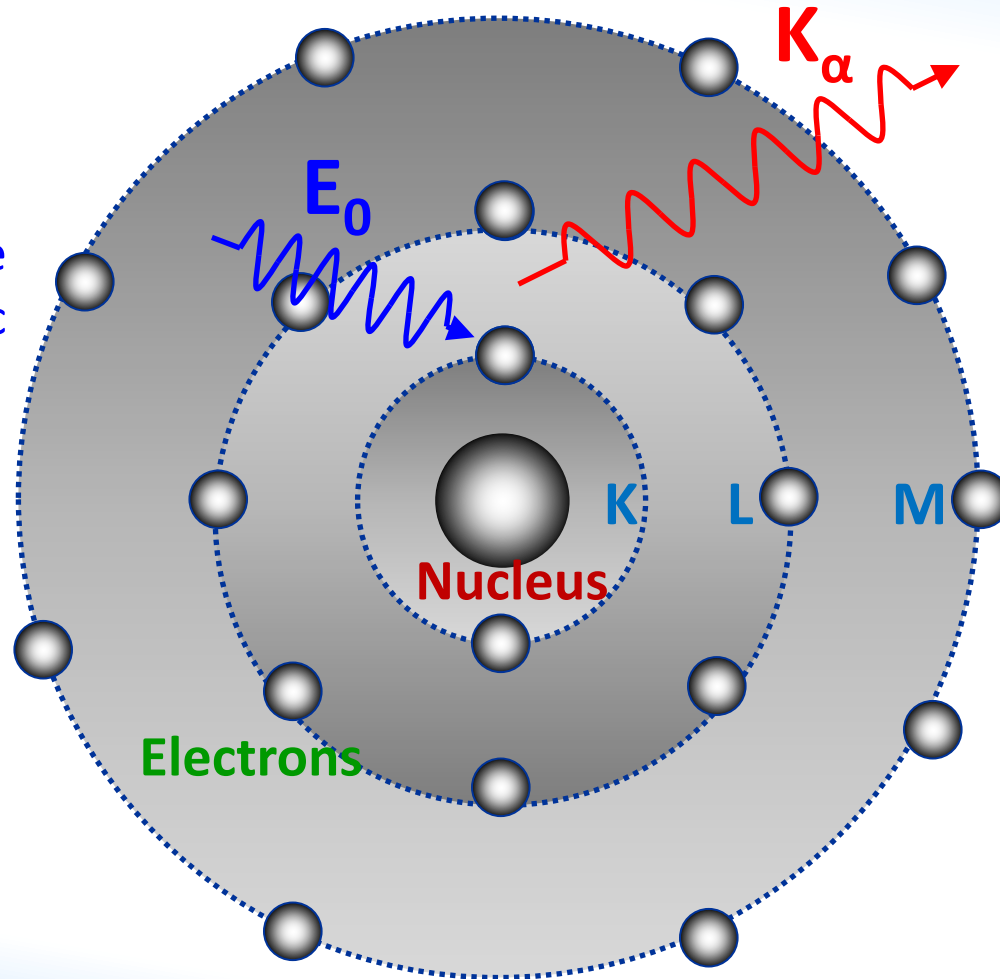
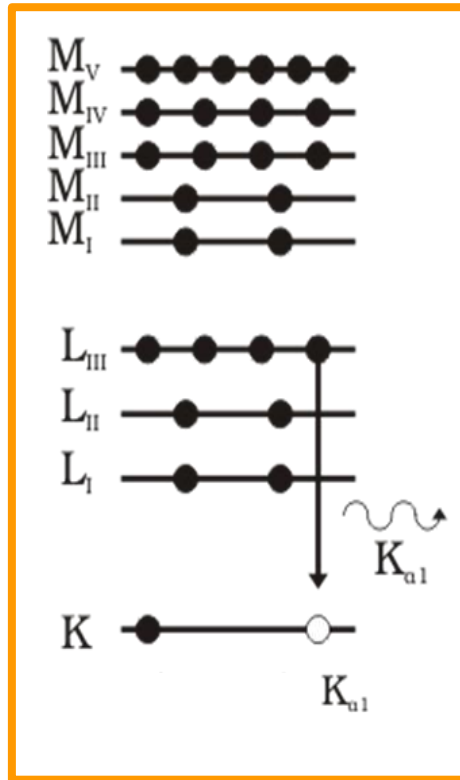


Photo-ionization  
of atomic bound  
electrons  
(K, L, M)  
(Photoelectric  
absorption)

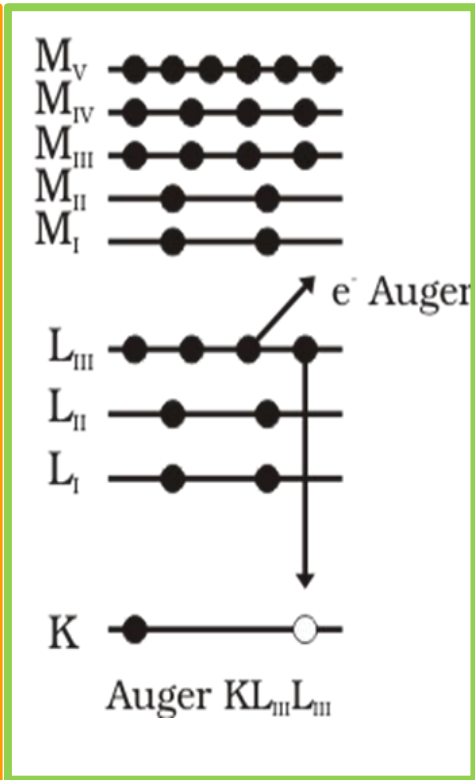
Electronic  
transition and  
emission of  
element  
→ **characteristic  
fluorescence  
radiation**

Fluorescence  
X-ray emission  
is **isotropic**

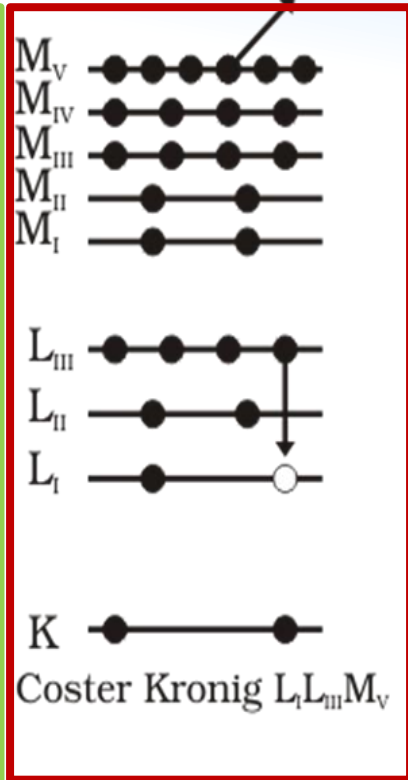
# □ De-excitation: Fluorescence/Auger



Emission of characteristic X-ray



Emission of electron (vacancy filled by electron from different shell)

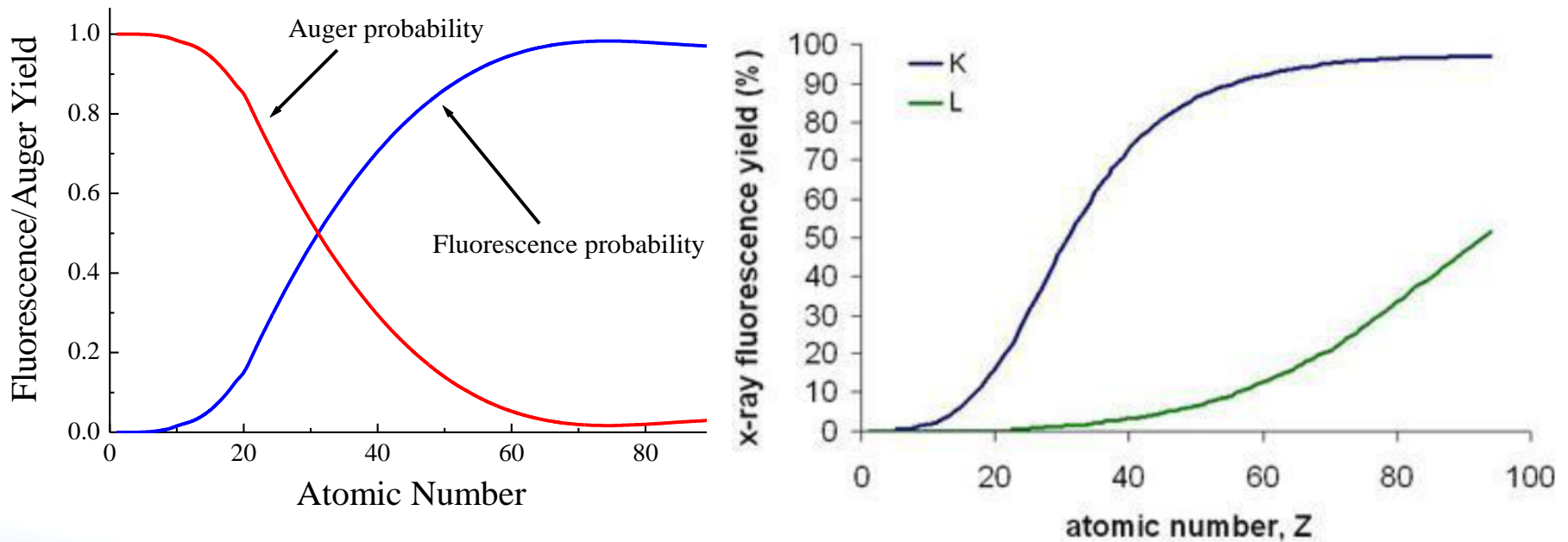


Emission of electron (vacancy filled by electron from the same shell)



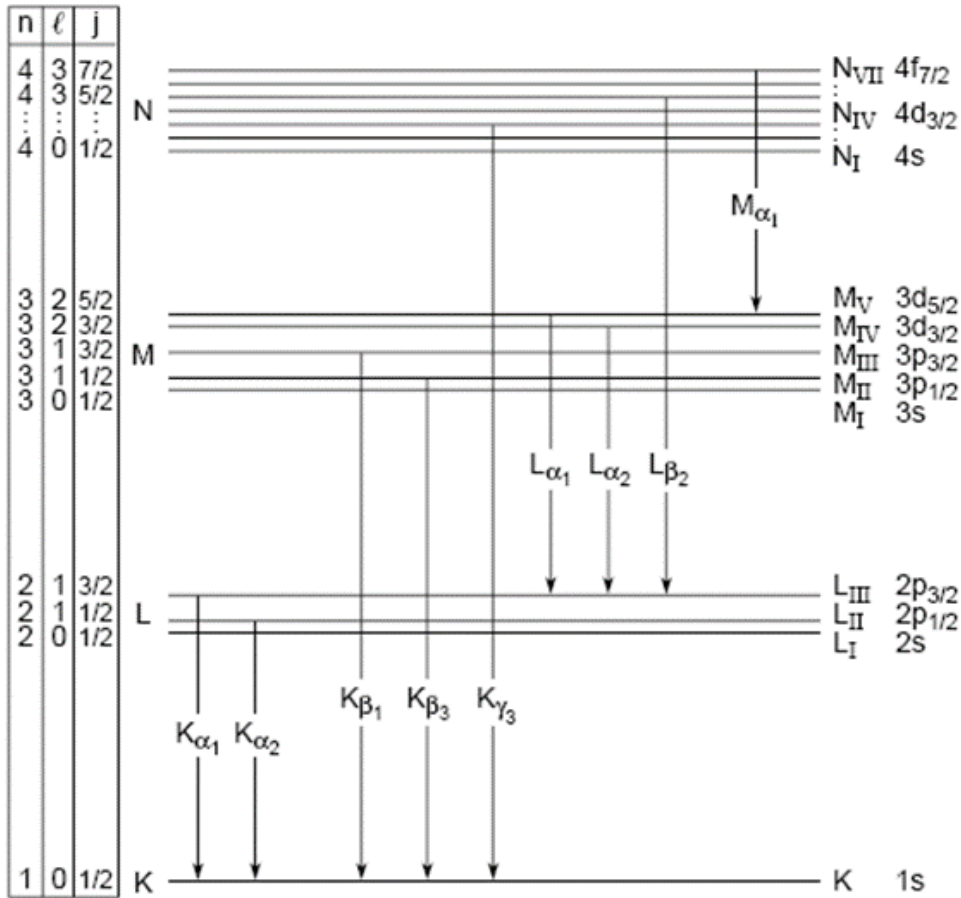
# Fluorescence yield

The fluorescence yield is given by the **ratio of the emitted fluorescence photons over the number of the created holes**. The competing process is the **emission of Auger electrons** as the atom returns to its ground state



**For low Z the Auger electron emission is dominant**

# □ Emission of characteristic X-rays



The emission of characteristic X-ray lines follows allowed electronic transitions between specific subshells. Each element has a unique set of emission lines.

## Siegbahn/IUPAC notation:

$K_{\alpha}$ : K-L<sub>2</sub> + K-L<sub>3</sub>

$K_{\beta}$ : K-M<sub>2</sub> + K-M<sub>3</sub>

$L_{\alpha}$ : L<sub>3</sub>-M<sub>4</sub> + L<sub>3</sub>-M<sub>5</sub>

$L_{\beta_1}$ : L<sub>2</sub>-M<sub>4</sub>

$L_{\beta_2}$ : L<sub>3</sub>-N<sub>5</sub>

# □ X-ray energies

Moseley's law

$$E = h \cdot A \cdot R \cdot (Z - b)^2$$

$h$  = Planck constant

$R$  = Rydberg frequency

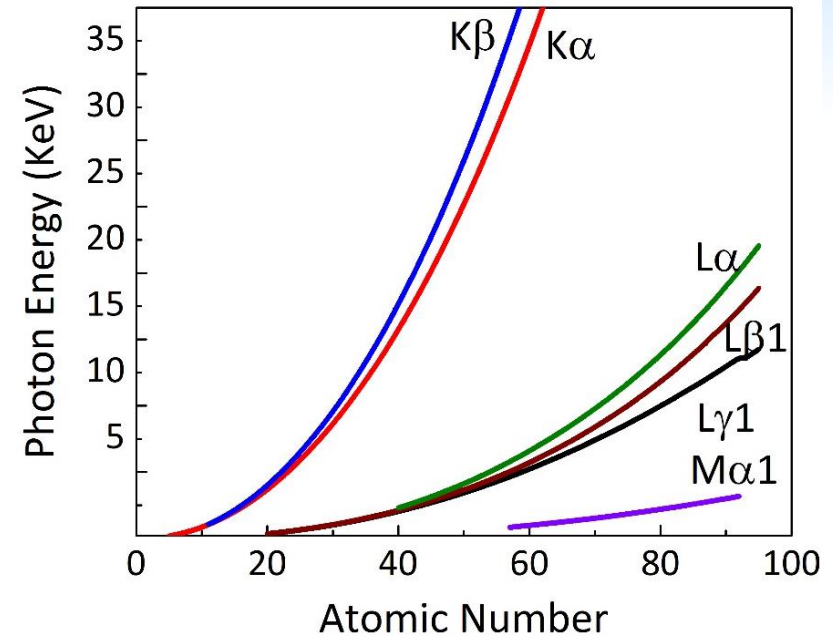
$Z$  = atomic number

$A = 3/4$  for  $K_\alpha$ ,  $5/36$  for  $L_\alpha$

$b = 1$  for  $K_\alpha$ ,  $7.4$  for  $L_\alpha$

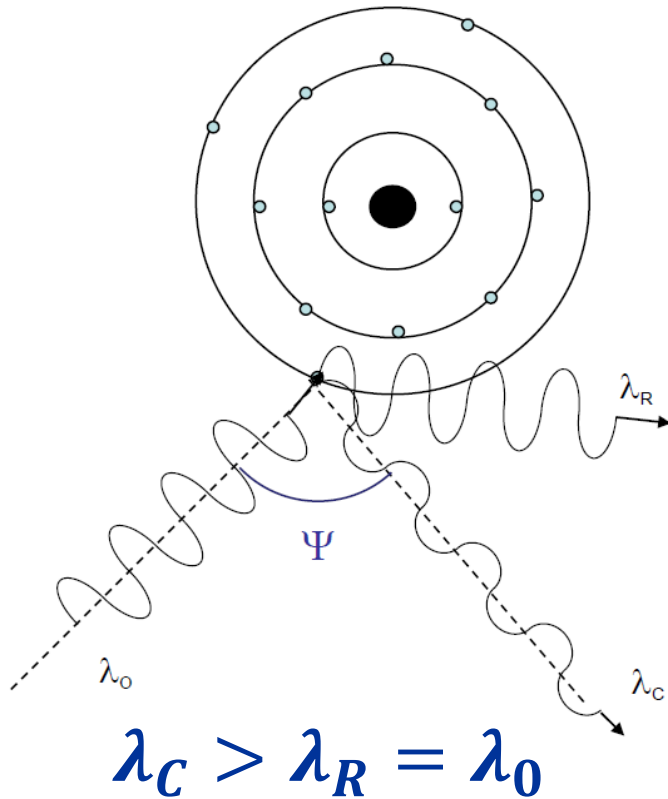
$K_\alpha$	$E \text{ [eV]} \approx 10.20 \cdot (Z - 1)^2$	$E_{Fe-K\alpha} \approx 6380 \text{ eV}$
------------	--	--

$L_\alpha$	$E \text{ [eV]} \approx 1.89 \cdot (Z - 7.4)^2$	$E_{Pb-L\alpha} \approx 10520 \text{ eV}$
------------	---	---



X-ray spectroscopy within the energy range 1÷30 keV offers in principle the possibility to detect all the periodic table elements ( $Z > 10$ ) through their K, L or even M series of emission lines

# □ X-ray scattering



## Elastic/coherent scattering (Rayleigh):

no energy loss after collision with electrons. The Rayleigh effect is present when electrons are strongly bound.

Rayleigh is more intense for high Z (= heavy) matrices

## Inelastic/incoherent scattering (Compton):

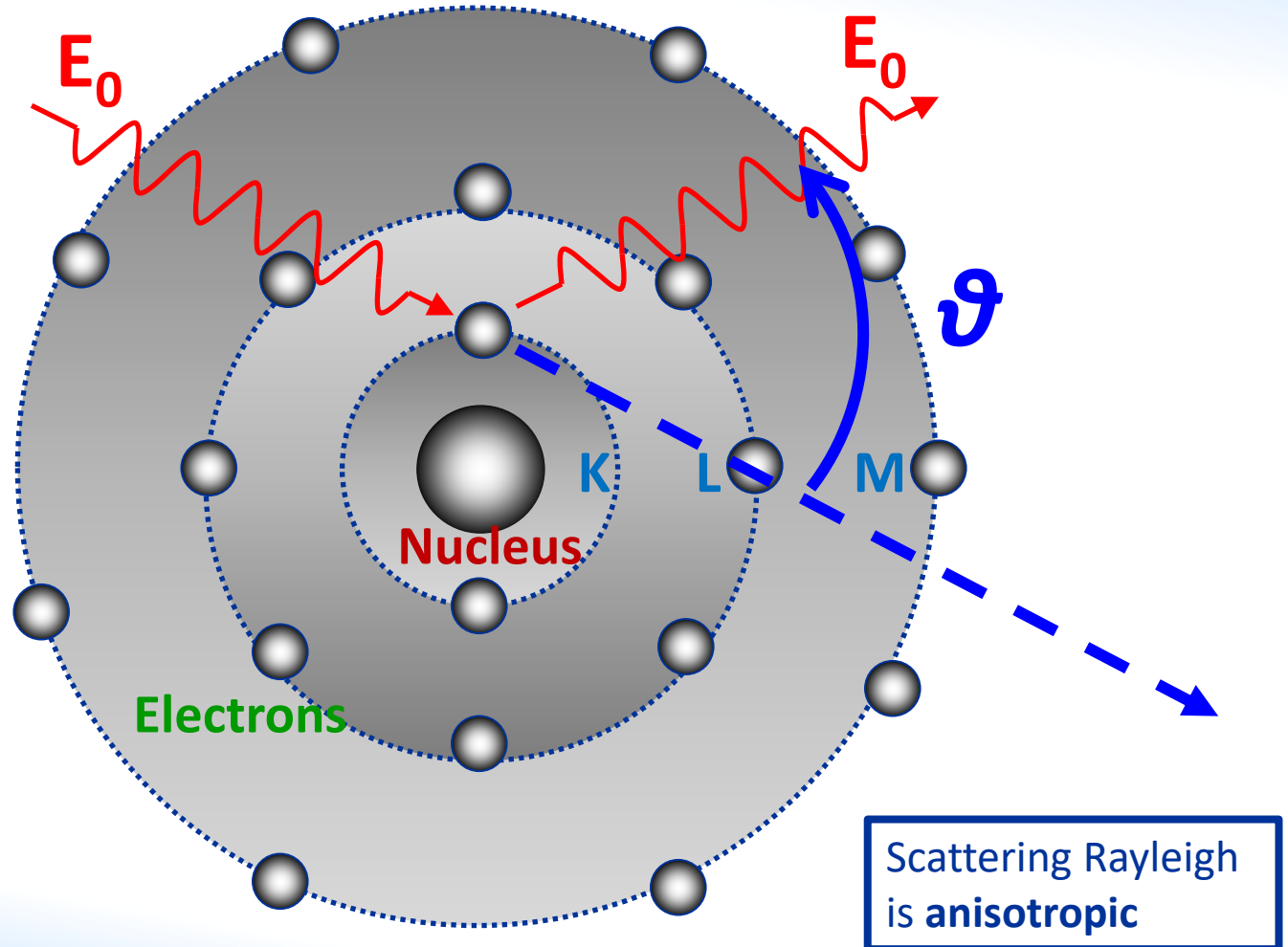
energy loss after collision with electrons. The Compton effect is present when electrons are loosely bound.

Compton is more intense for low Z (= light) matrices

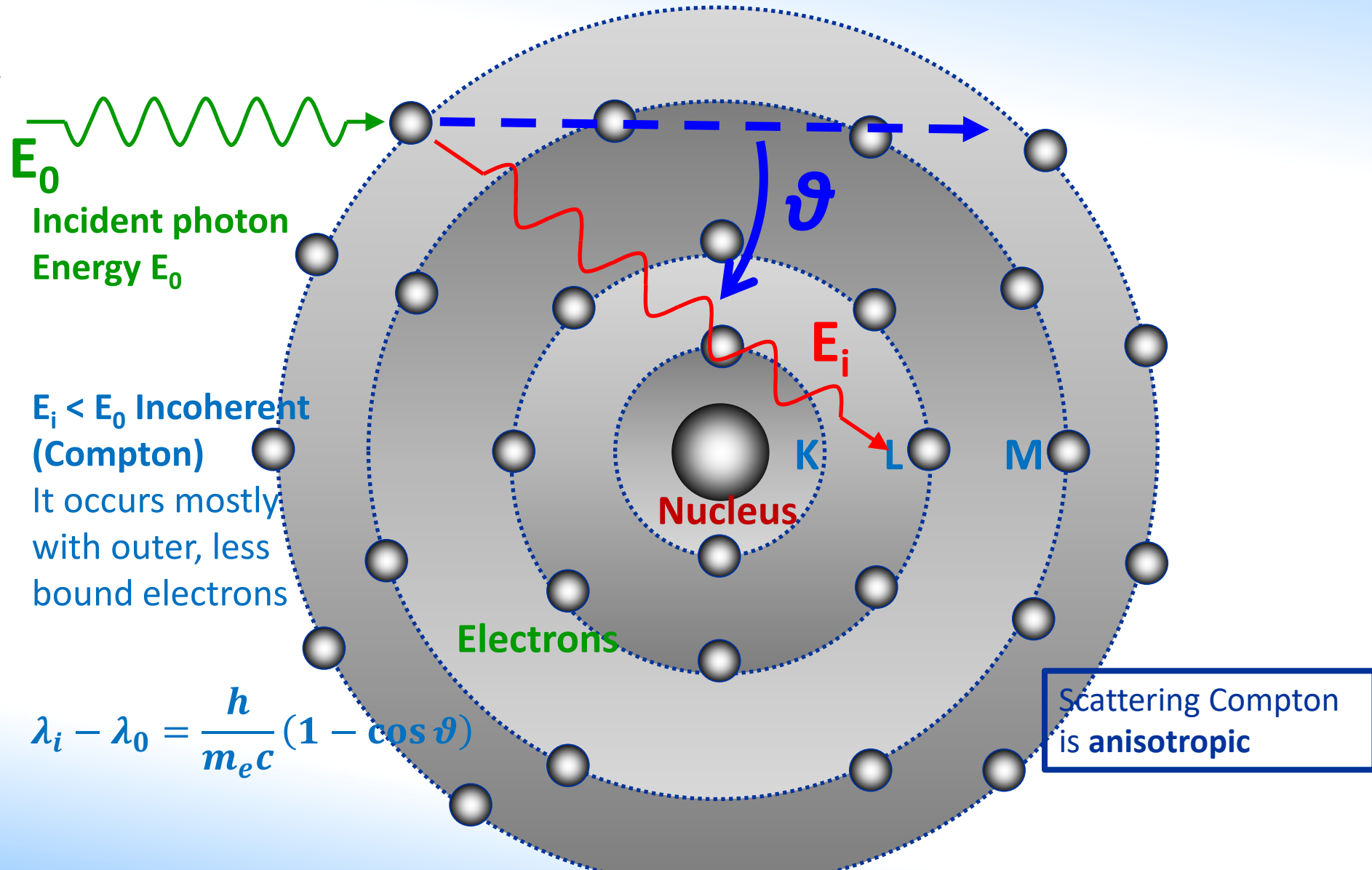
# □ Rayleigh scattering

Incident photon  
Energy  $E_0$

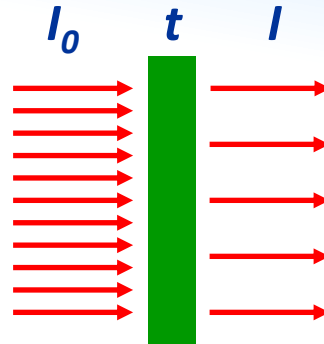
$E_i = E_0$  : Coherent  
(Rayleigh)  
It occurs mostly  
with inner atomic  
electrons



# Compton scattering



# □ Linear attenuation coefficient $\mu$



Attenuation of photons by a thin layer of thickness  $dt$  is described by

$$dI = I \cdot \mu \cdot dt$$

where  $I$  is the number of photons per unit area and unit time (photon flux) of which  $dI$  are attenuated while penetrating the layer of a material characterized by the **(total, linear) attenuation coefficient  $\mu$** . This is equivalent to

$$I = I_0 \cdot e^{-\mu \cdot t}$$

$I$  and  $I_0$  are the photon fluxes behind and in front of the absorber, respectively, and  $t$  is the thickness.  $\mu$  is a function not only of the material (atomic number  $Z$ ) but also of the photon energy  $E$

# □ Mass attenuation coefficient $\mu_m$

$$\mu = \mu_m \cdot \rho$$

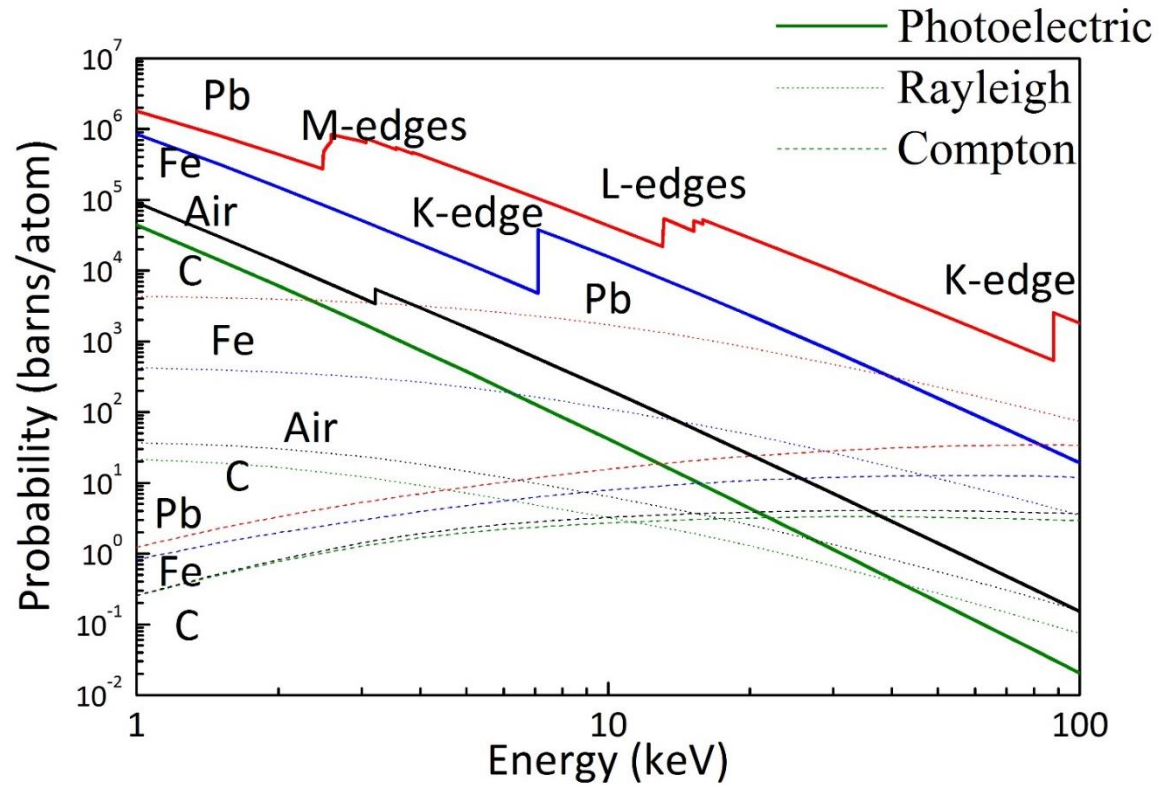
the total mass attenuation coefficient  $\mu_m$  doesn't depend on the density  $\rho$  of the material.

The coefficient  $\mu_m$  summarizes all possible photon interactions

$$\mu_m = \tau_m + \sigma_m$$

where  $\tau_m$  describes the photo absorption and  $\sigma_m = \sigma_{coh} + \sigma_{inc}$  are the contributions by coherent and incoherent scattering, respectively.

Both kinds of scattering contribute much less than the photo absorption to the total  $\mu_m$





# □ Mass attenuation coefficient $\mu_m$

the mass attenuation coefficient of a material that is composed of several elements, with weight fractions  $w_i$ , is

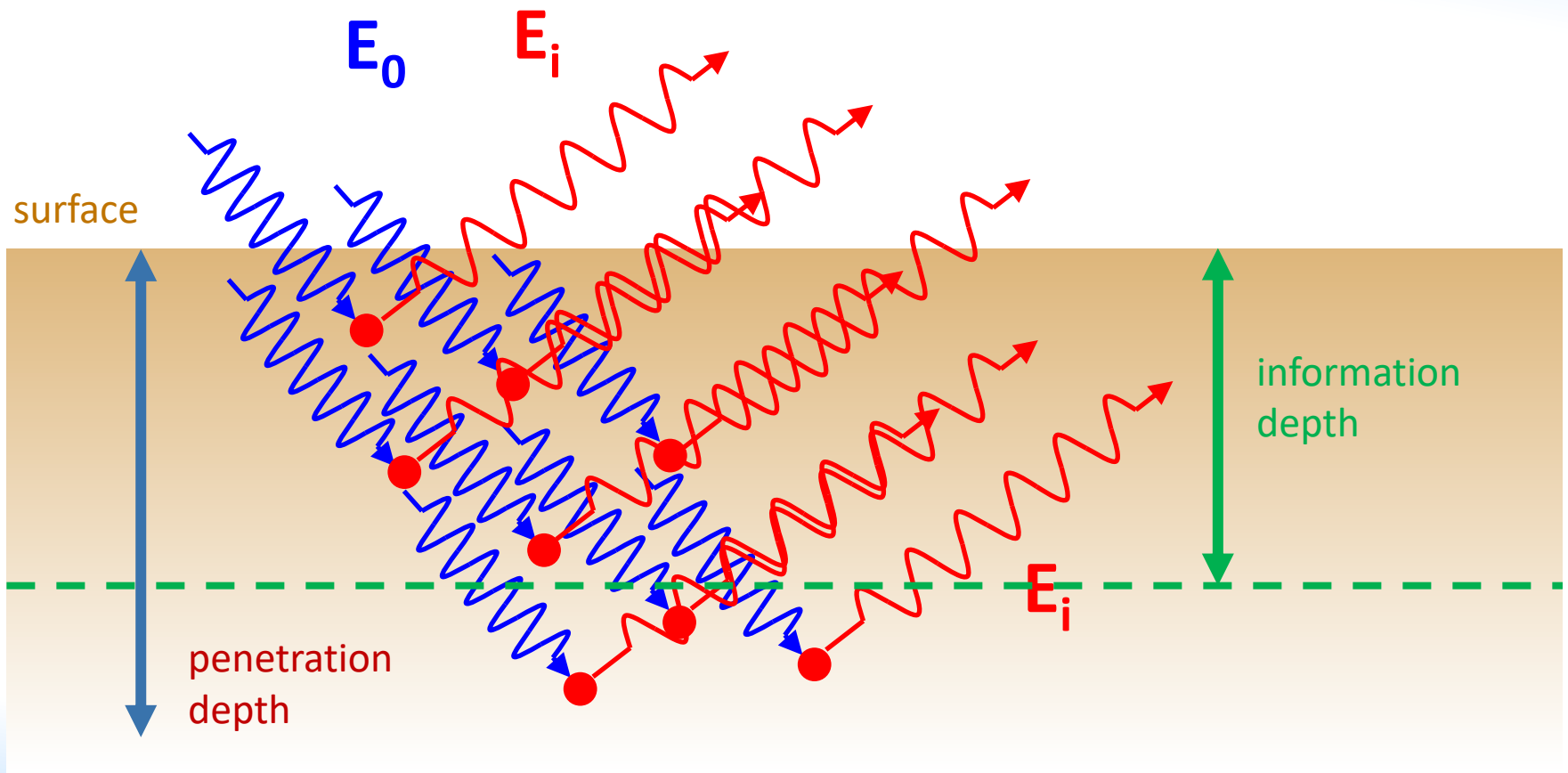
$$\mu_m = \sum_i w_i \cdot \mu_m^i$$

Use of mass attenuation coefficients suggests replacing the thickness by the **area-related mass**  $m = M/A$  (mass  $M$  per unit area  $A$ ) and rewriting the attenuation law as

$$I = I_0 \cdot e^{-\mu_m \cdot m}$$

$t \cdot \rho = M/A$ , in **grams/cm<sup>2</sup>**

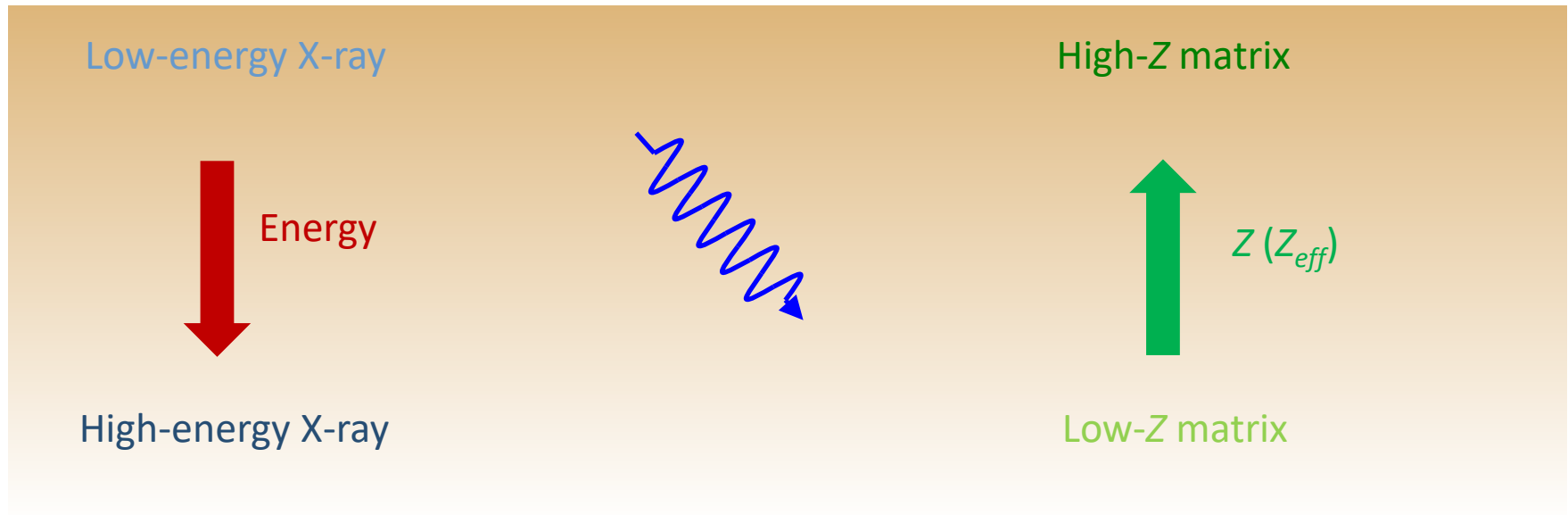
# □ Penetration and information depth



# □ Penetration and information depth

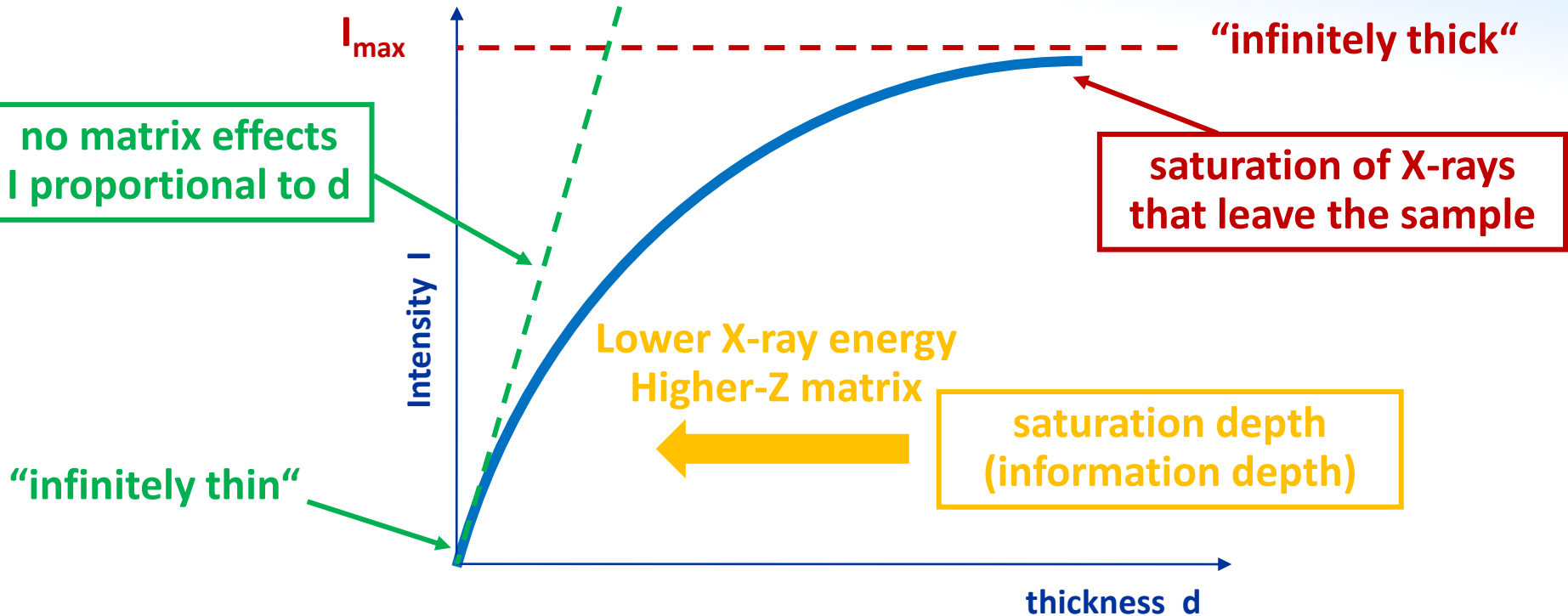
Penetration and information (analytical) depth depend on the energy of the X-ray and on the matrix:

surface



- Surface treatment is extremely important for heavy matrices
- Information thickness is essential for light matrices

# □ Influence of sample thickness



Increasing the thickness of the sample above the information depth will not increase the signal but only the scattering of the primary radiation

# □ Analytical depths in different matrices

Different elements exhibit different Information thicknesses (99%), depending on their characteristic X-ray energy and on the overall matrix

Line	Energy	Graphite	Glass	Iron	Lead
Cd K <sub>α1</sub>	23,17 keV	14,46 cm	8,20 mm	0,70 mm	77,30 μm
Mo K <sub>α1</sub>	17,48	6,06	3,60	0,31	36,70
Cu K <sub>α1</sub>	8,05	5,51 mm	0,38	36,40 μm	20,00
Ni K <sub>α1</sub>	7,48	4,39	0,31	29,80	16,60
Fe K <sub>α1</sub>	6,40	2,72	0,20	*164,00	11,10
Cr K <sub>α1</sub>	5,41	1,62	0,12	104,00	7,23
S K <sub>α1</sub>	2,31	116,00 μm	14,80 μm	10,10	4,83
Mg K <sub>α1</sub>	1,25	20,00	7,08	1,92	1,13
F K <sub>α1</sub>	0,68	3,70	1,71	0,36	0,26
N K <sub>α1</sub>	0,39	0,83	1,11	0,08	0,07
C K <sub>α1</sub>	0,28	*13,60	0,42	0,03	0,03
B K <sub>α1</sub>	0,18	4,19	0,13	0,01	0,01

$$E_{Kc} = 0.2842$$

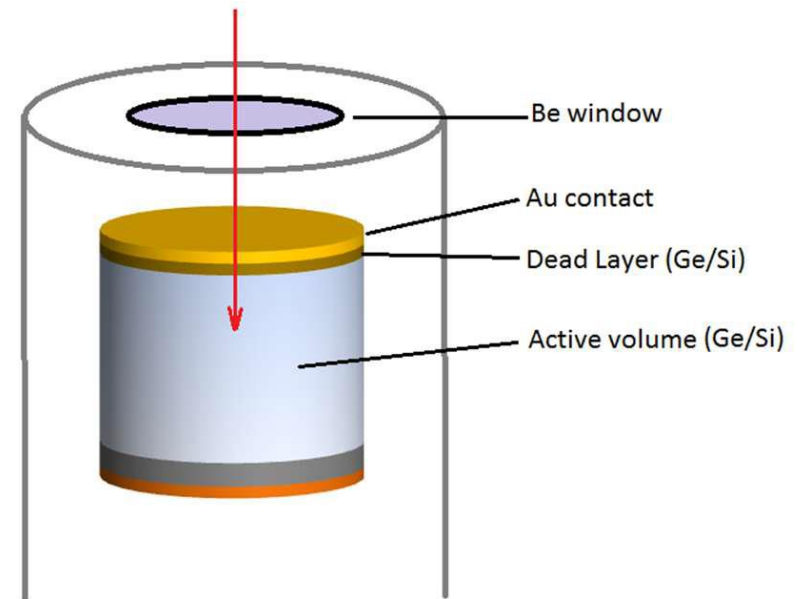
$$E_{KFe} = 7.112$$

# Detectors

- Proportional Counters
- Scintillation Detectors
- Si(Li)
- LEGe
- PIN Diode
- **SDD**
- CCD, CMOS cameras
- CZT, other

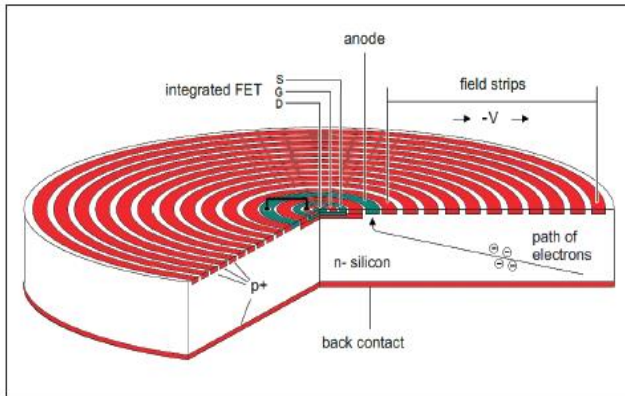
# □ Semiconductor detectors

- X-rays produce **electron-hole pairs**, whose number is **proportional** to the energy of the radiation (average energy to produce an electron/hole pair is 3.6eV for Si and 2.9eV for Ge)
- Electrons and holes are collected from the depleted active region to the electrodes, where they result in a **pulse** that can be further **amplified** and finally **measured**
- This pulse carries information about the energy of the original incident radiation. The number of such pulses per unit time also gives information about the intensity of the radiation



# □ Silicon Drift Detectors - SDD

The charge is drifted from a large area into a small read-out node with low capacitance, independent of the active area of the sensor. Thus, the serial noise decreases, and shorter shaping time can be used. For SDDs faster counting is enabled and higher leakage current can be accepted, drastically reducing the need for cooling.



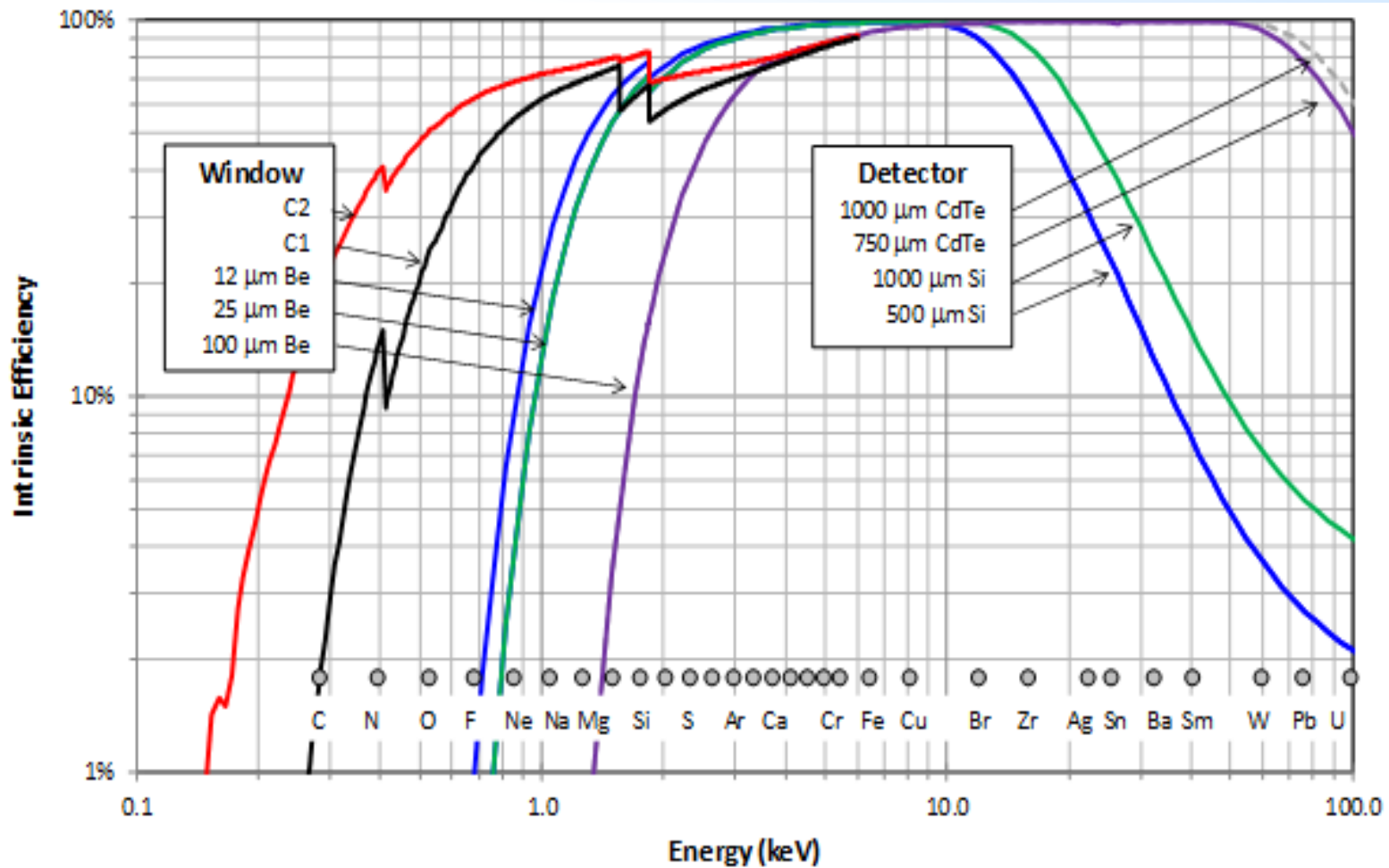
- Energy resolution  $\sim 125 - 140$  eV (Mn-Ka)
- Input capability  $\sim 10^6$  photons/sec

[https://tools.thermofisher.com/content/sfs/brochures/TN52342\\_E\\_0512M\\_SiliconDrift\\_H.pdf](https://tools.thermofisher.com/content/sfs/brochures/TN52342_E_0512M_SiliconDrift_H.pdf)

Detector photograph reproduced from <https://www.rayspec.co.uk/x-ray-detectors/silicon-drift-detectors/xrf/>



# Efficiencies of different detectors

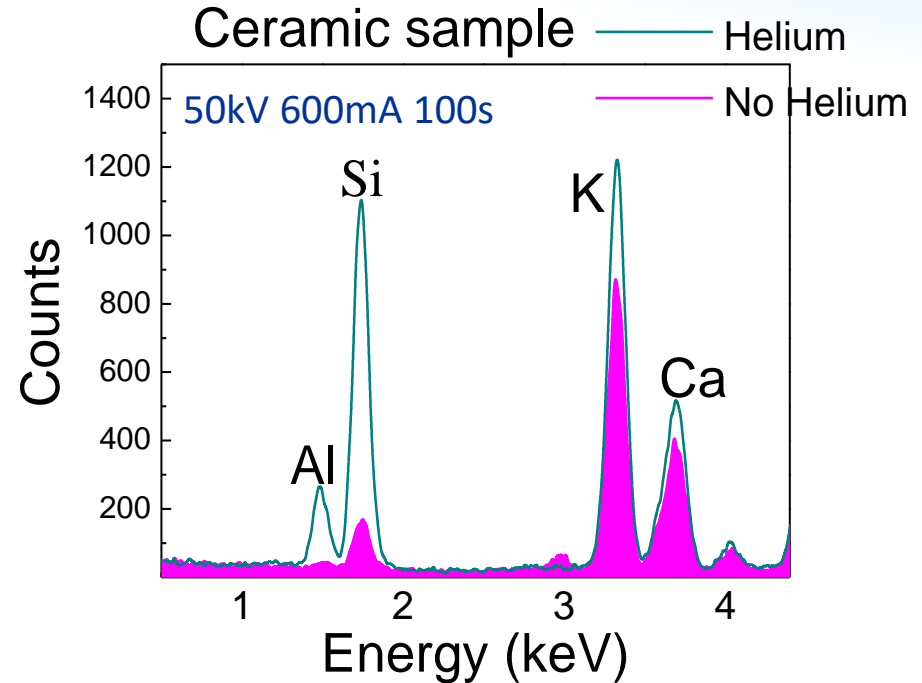
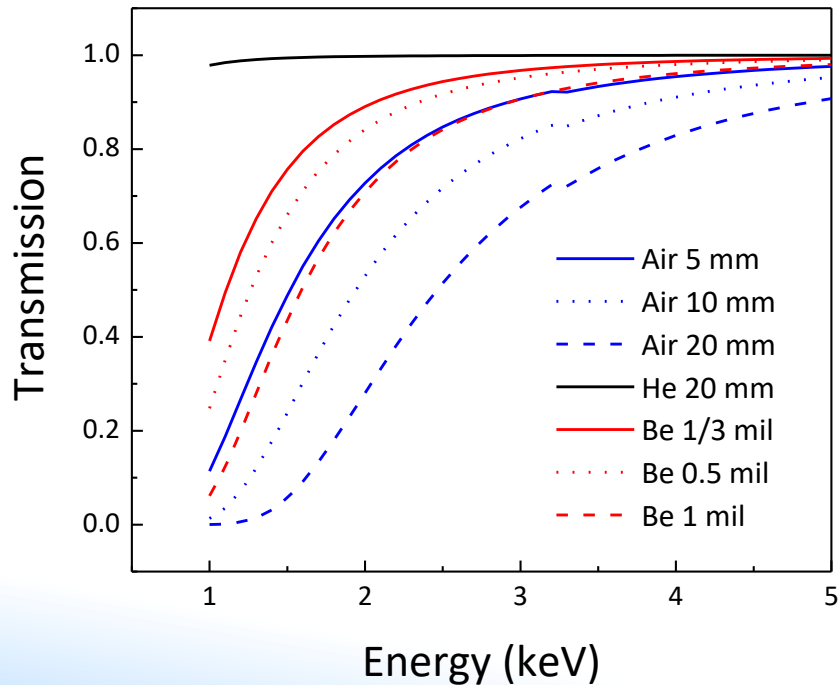


Comparison of different detector's efficiency from AMPTEK

<https://www.amptek.com/products/x-ray-detectors/faststd-x-ray-detectors-for-xrf-eds/faststd-silicon-drift-detector>

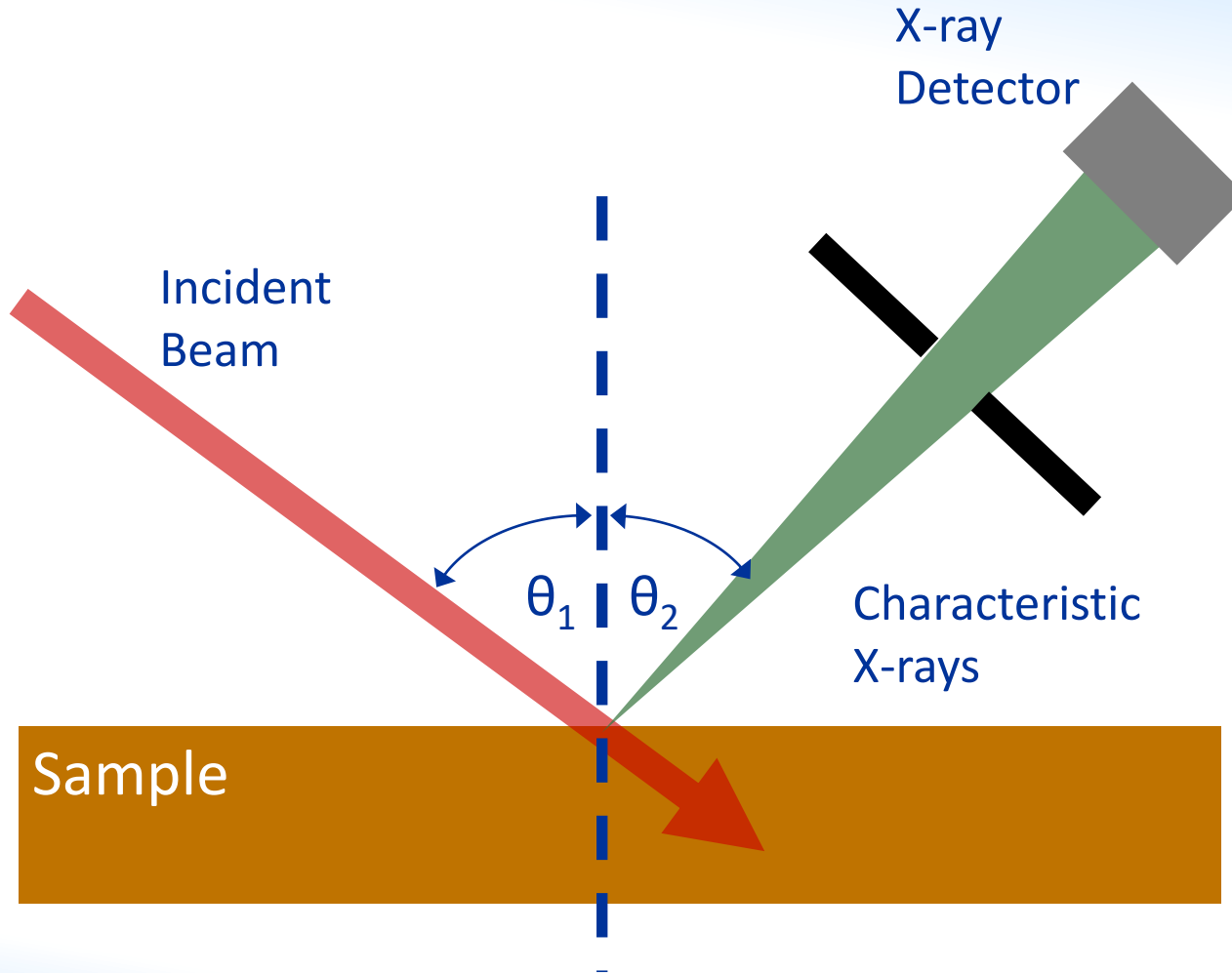
# ☐ “Light” elements (Na, Mg, Al, Si)

**Vacuum atmosphere or He flushing** is required in the x-rays path between sample and detector



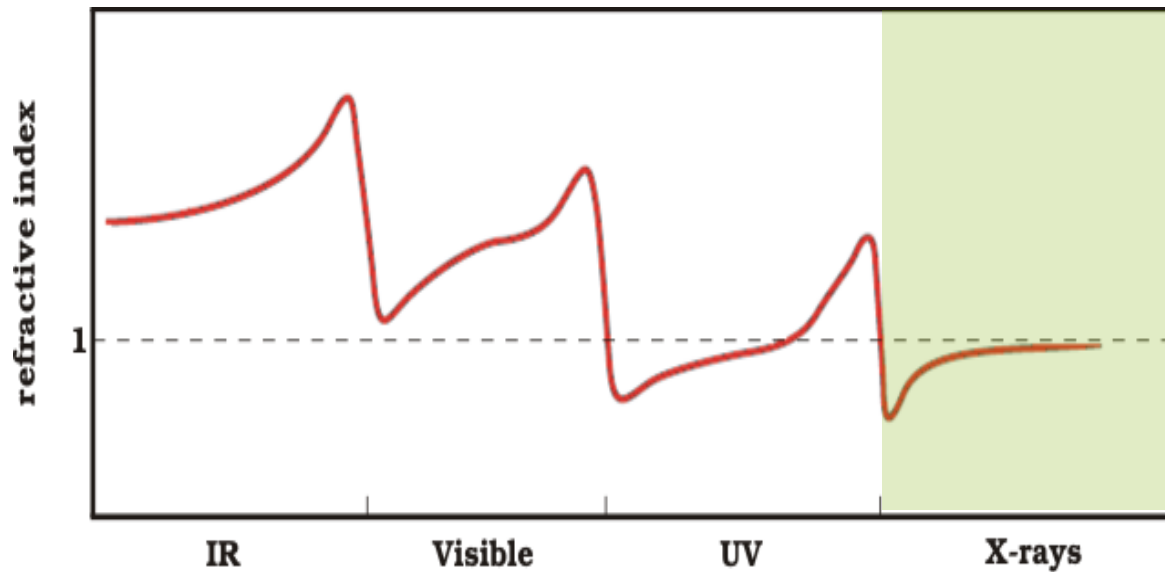
The improvement in the intensity of Al-K and Si-K characteristic X-ray lines is significant, 22 and 7.3 times respectively

# Conventional XRF



# X-ray optics

Refractive index:  $n = \frac{c}{u_p}$

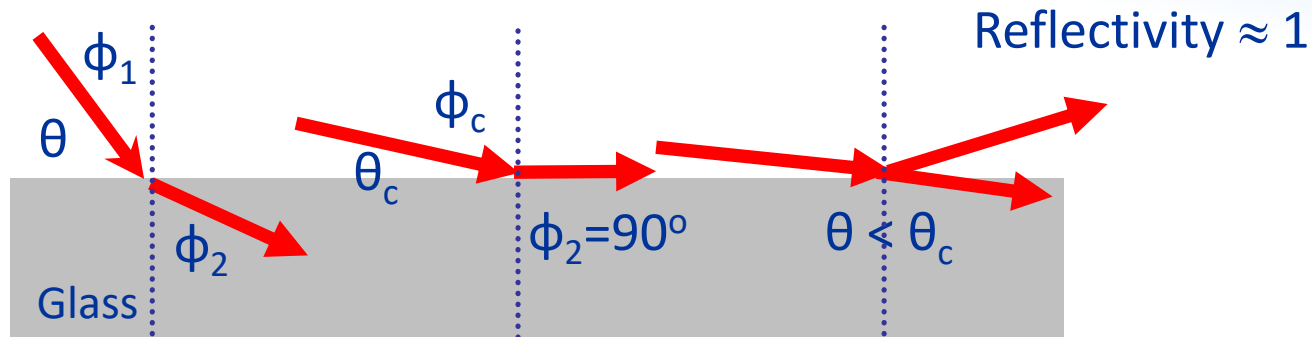


$$n = 1 - \delta + i\beta$$

$\beta$  = Attenuation term

$\delta$  = Phase term

# □ X-ray total reflection

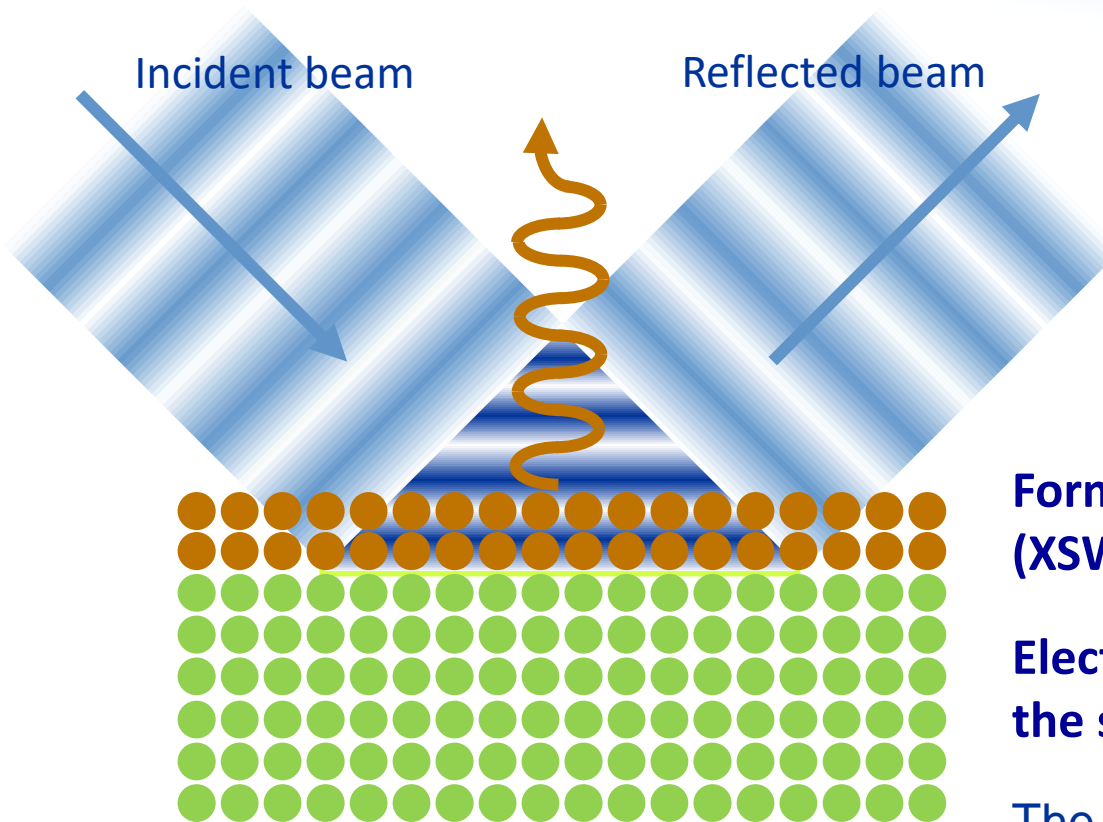


Snell Law  $\frac{\sin \phi_2}{\sin \phi_1} = \frac{1}{n} \Rightarrow \sin \phi_2 = \frac{\sin \phi_1}{n} \Rightarrow \phi_2 > \phi_1 \quad n \approx 1 - \delta$

$$\vartheta_{crit} = \sqrt{2\delta} \quad \vartheta_{crit} (deg) \approx \frac{1.651}{E(keV)} \sqrt{\frac{Z}{A} \rho \left( \frac{g}{cm^3} \right)}$$

Z: Atomic number  
 A: Atomic mass  
 $\rho$ : Density

# □ X-ray Standing Wave



**Formation of X-ray Standing Wave (XSW) at grazing incident/exit angle**

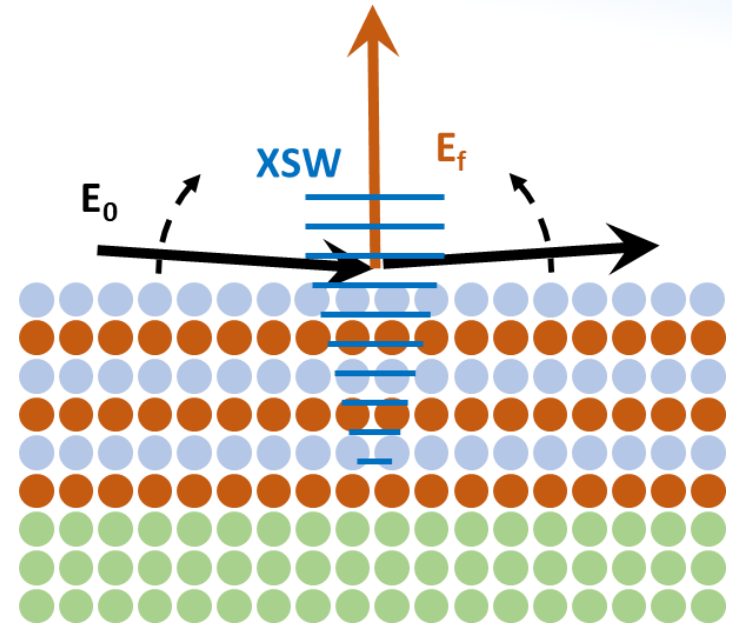
**Electric Field Modulations above the surface**

The X-ray fluorescence intensity from the sample depends on the varying field intensity of the XSW field within the sample

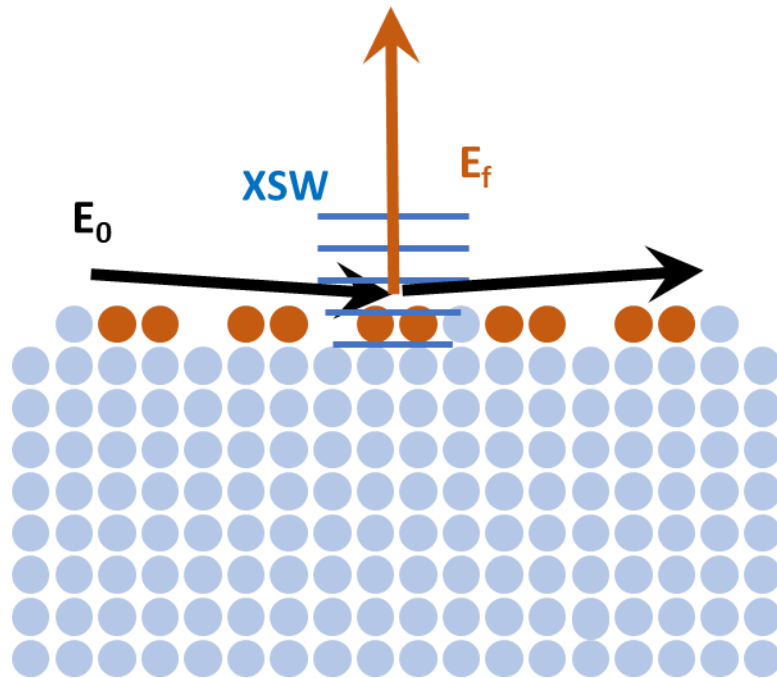
# □ GIXRF and XRR

By varying continuously the grazing incident angle through and few times above the critical angle for TR, the recorded XRF intensity profiles (Grazing Incidence-XRF analysis) have the potential to provide information on structural and compositional properties of thin films, such as the layer composition, sequence, thicknesses and densities, interface roughness, in depth elemental gradients of matrix elements or dopants in semiconductors, characterization of nano-particles deposited on flat surfaces, etc

A more accurate and robust reconstruction of these thin film properties requires the synergy or even the simultaneous fitting of GI-XRF with X-ray reflectometry (XRR) data



# □ Total reflection X-ray Fluorescence



TXRF is essentially an energy dispersive XRF technique arranged in a special geometry.

Due to this configuration, the measured spectral background in TXRF is less than in conventional XRF. This reduction results in increased signal to noise ratio.

TXRF is a surface elemental analysis technique often used for the ultra-trace analysis of particles, residues, and impurities on smooth surfaces.





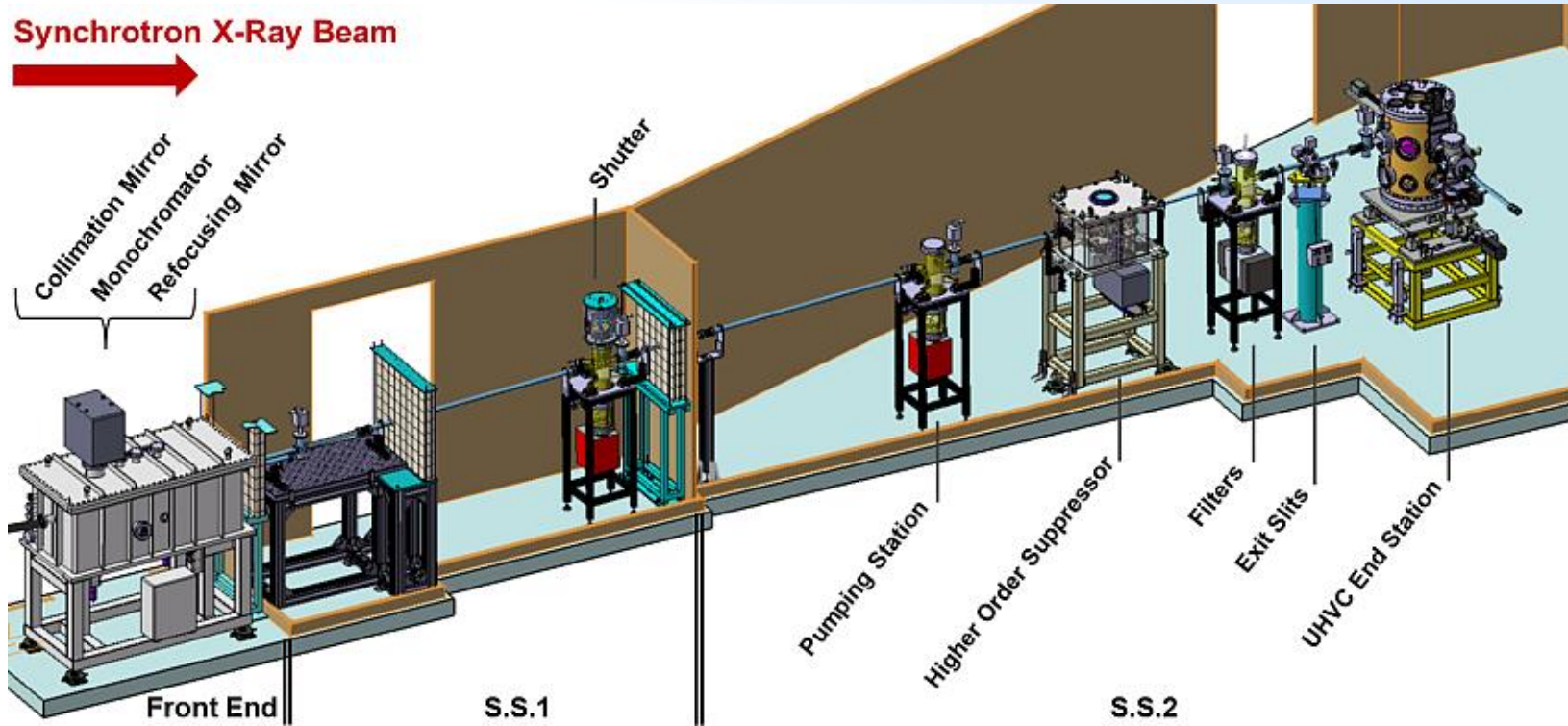
**IAEA**

International Atomic Energy Agency

# The joint IAEA-Elettra XRF beamline at Elettra Sincrotrone Trieste



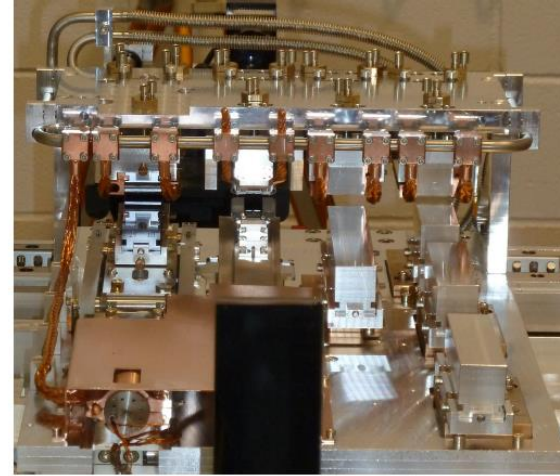
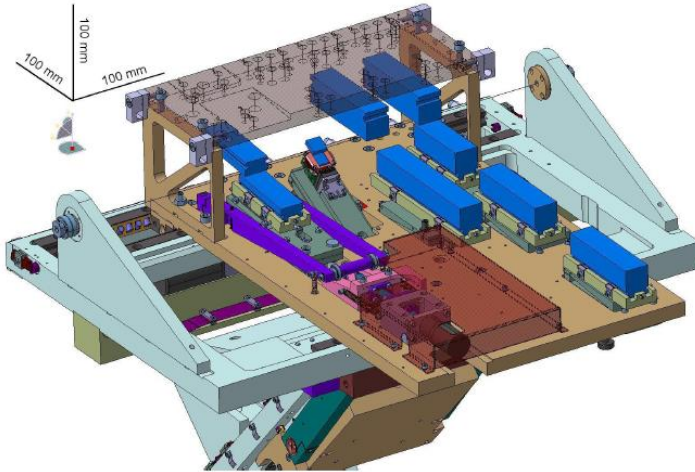
# Optical layout



Source	Bending magnet
Flux	$10^{10}$ ph/s (at 5 keV for 2.0 GeV, at 10 keV for 2.4 GeV) (Si 111)
Spot size	<b>250 x 100 (H x V) <math>\mu\text{m}^2</math></b>
Beam divergence	< 0.15 mrad (at exit slits)

Werner Jark, Diane Eichert, Lars Luehl, Alessandro Gambitta, *Optimisation of a compact optical system for the beam transport at the x-ray fluorescence beamline at Elettra for experiments with small spots*, Proc. SPIE 9207, Advances in X-Ray/EUV Optics and Components IX, 92070G, 2014; doi: 10.1117/12.2063009

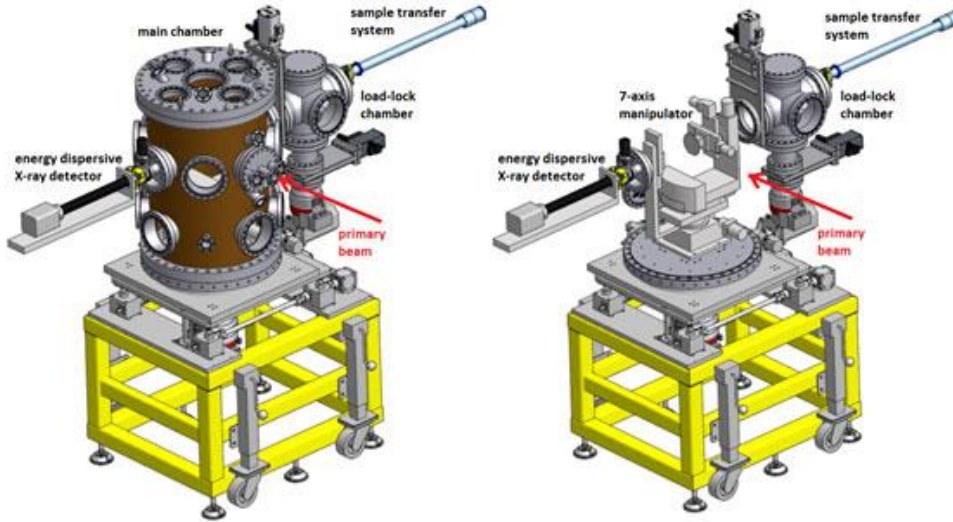
# □ The monochromator at XRF



Optics type	E range (keV)	E resolution ( $\Delta E$ )
Si(111)	3.6 - 14	~ 1 eV at 7 keV
InSb(111)	2.0 – 3.8	~ 1eV at 2.2 keV
ML: High E (RuB <sub>4</sub> C)	4.0 – 14.0	~ 55 eV at 1 keV ~ 180 eV at 14 keV
ML: Medium E (NiC)	1.5 – 8.0	
ML: Low E (RuB <sub>4</sub> C)	0.7 – 1.8	

Werner Jark *et al.*, Proc. SPIE 9207, Advances in X-Ray/EUV Optics and Components IX, 92070G, 2014; doi: 10.1117/12.2063009

# IAEXspe endstation

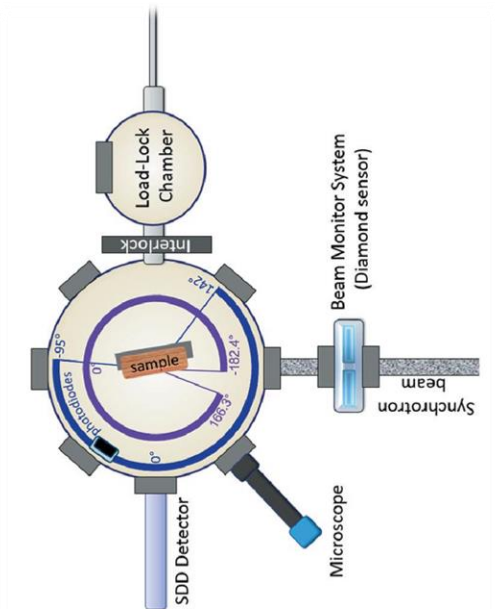


The IAEA end-station is based on a prototype design by Physikalisch - Technische Bundesanstalt (PTB, Berlin) and Technical University of Berlin (TUB)

## Available detectors:

- Diamond detector for  $I_0$
- SDD detector for **XRF** (different variants) and **XAS** (in fluorescence geometry)
- Photodiodes for **XAS** in transmission geometry
- Photodiodes with 100 and 200 $\mu\text{m}$  slits and SDD for **XRR**

Andreas G. Karydas et al., J. Synchrotron Rad. (2018). 25, 189–203



# □ 7-Axis Manipulator

## Sample arm

- 3 linear stages (X, Y, Z)
- 2 goniometers (Theta, Phi)

## Photodiodes arm:

- 1 linear stages (diode)
- 1 goniometer (2Theta)

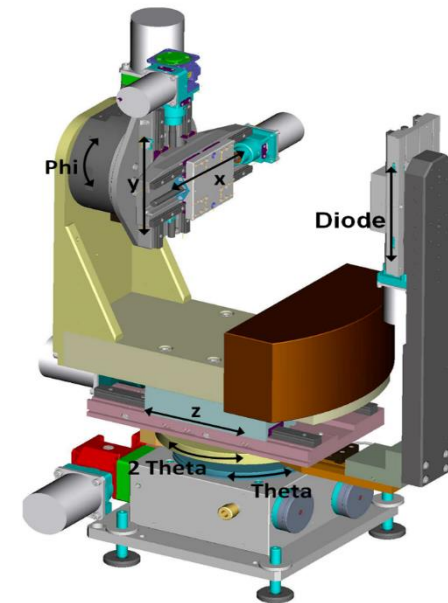
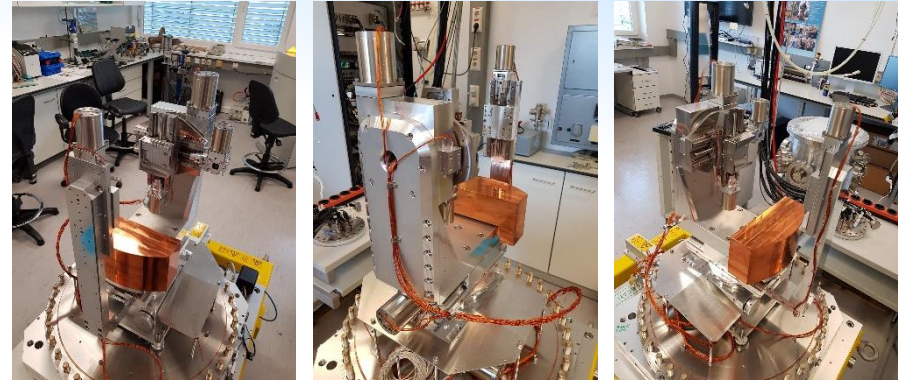
- Sample can be moved in various directions/orientations with respect to the exciting X-ray beam or with respect to the detectors.

- Ultra Thin Window (UTW) Bruker Silicon Drift detector (30 mm<sup>2</sup>, FWHM 131 eV @ Mn-Ka), Si photodiodes

## Full step resolution

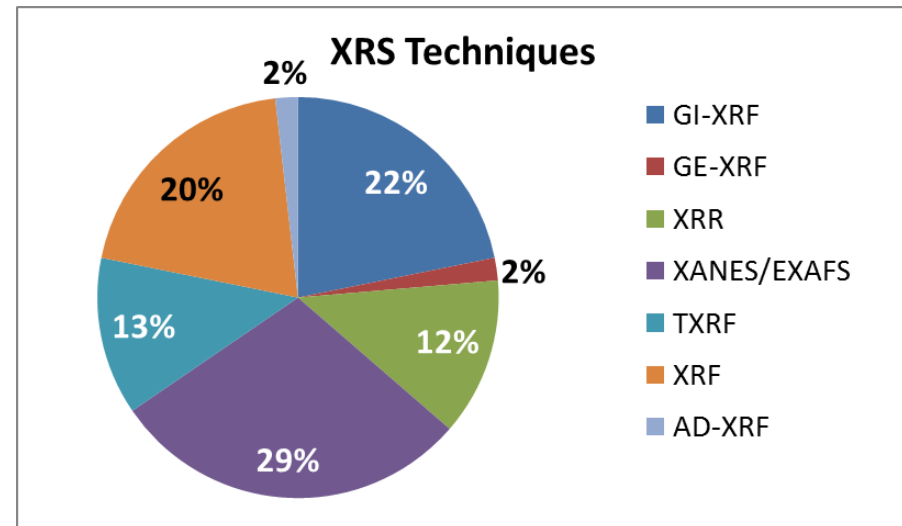
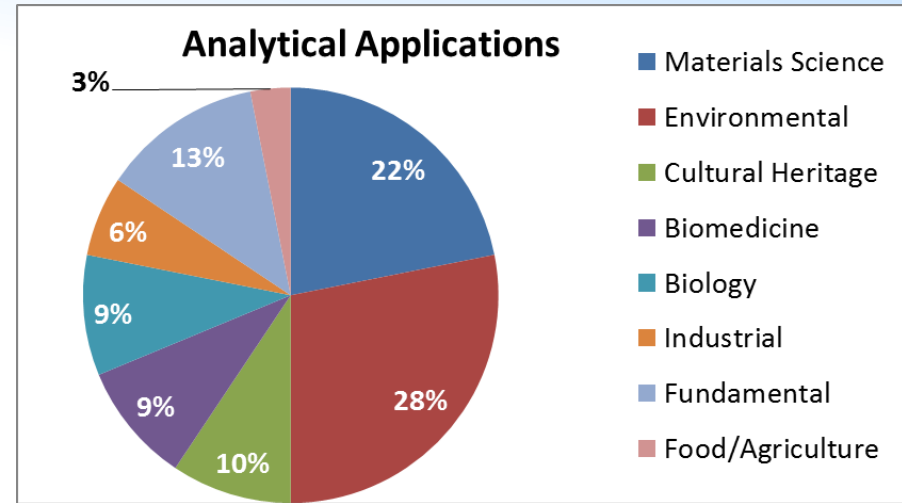
Linear axes: Diode, X, Y, Z (0.005mm, 0.005mm, 0.0005mm, 0.01mm)

Goniometers: Theta, 2theta, phi (0.001°, 0.001°, 0.005°)

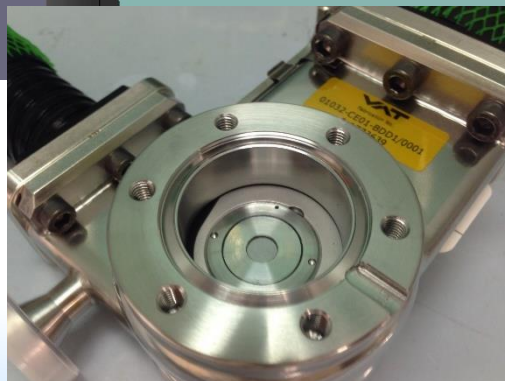
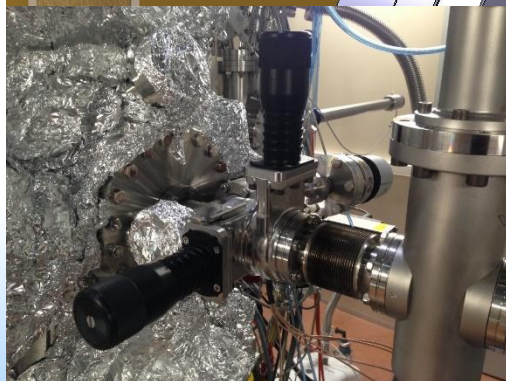
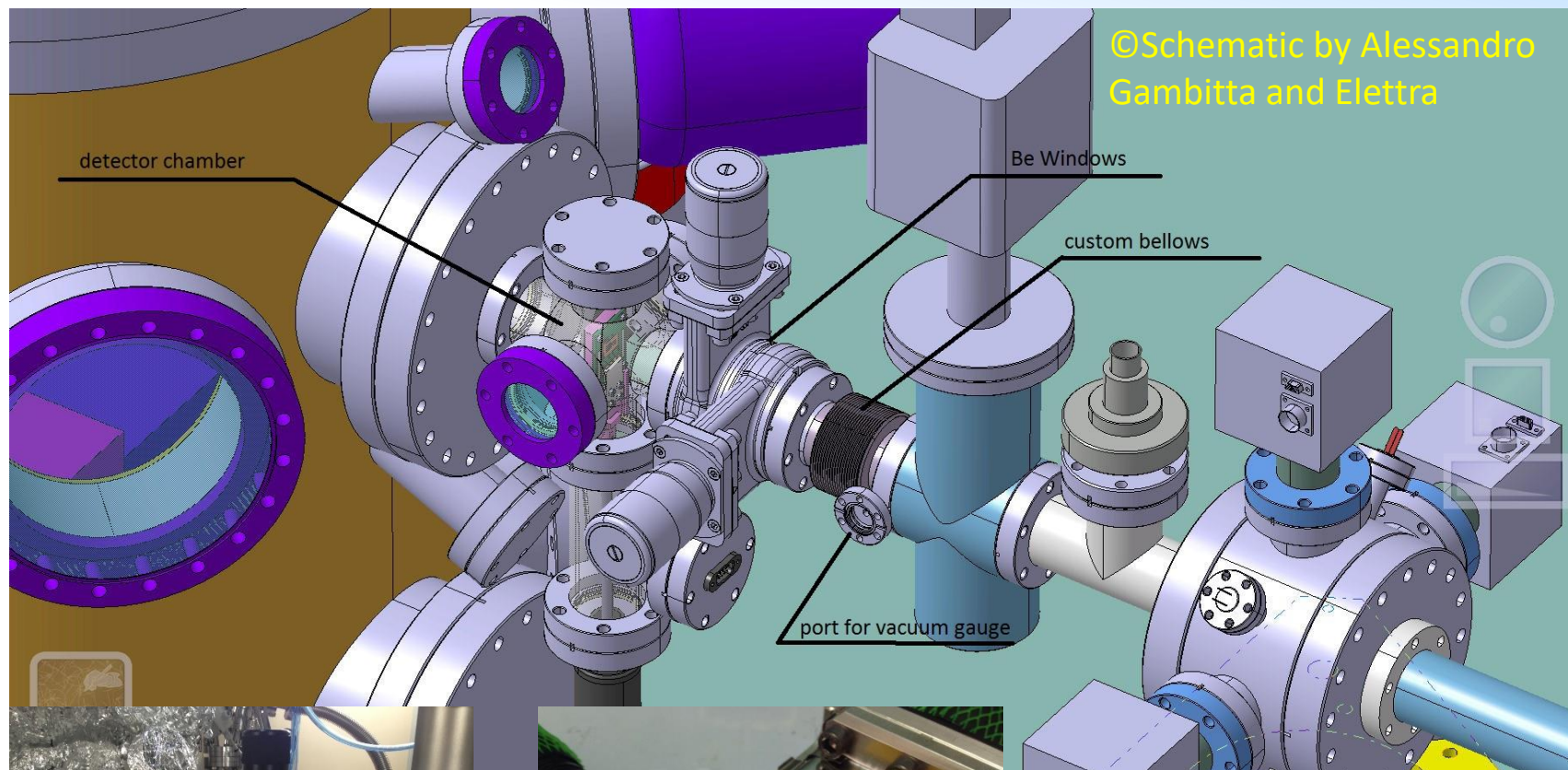


# IAEA Coordinated Research Project

- **Materials Science:** Structured materials for energy storage and conversion technologies
- **Nanomedicine - Biosensing technologies**
- **Environmental monitoring** (air particulate matter, water)
- **Biological:** Elemental distribution/speciation on plant organ (leaves, roots, shoots, seeds, etc.)
- **Cultural Heritage –preventive conservation**
- **Food products security – Authenticity**
- **Determination of X-Ray Fundamental Parameters**

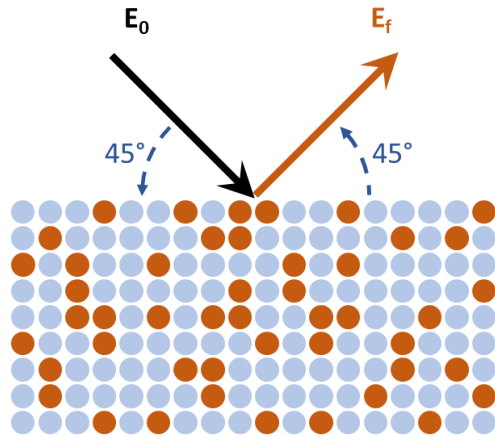


# ☐ non-UHV compatible samples



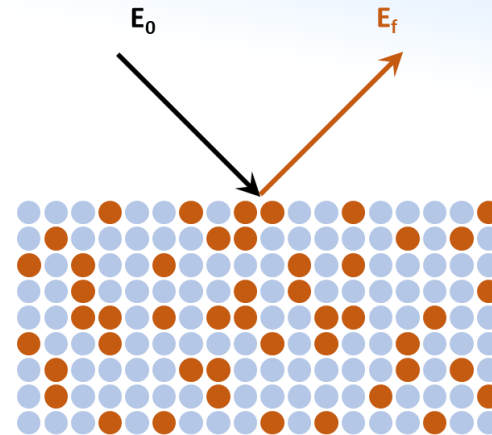
**20 $\mu$ m IF-1 Beryllium  
Luxel Corporation**

# Geometries and techniques



Standard 45°/45° - XRF

Elemental characterization



micro - XRF

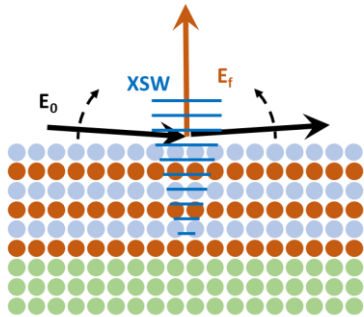
Mapping



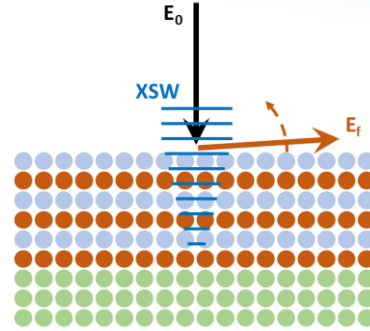
X-ray Absorption Spectroscopy  
(on hot spots)



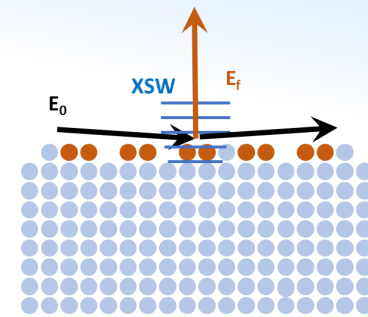
# Grazing angle geometries



Grazing Incident - XRF



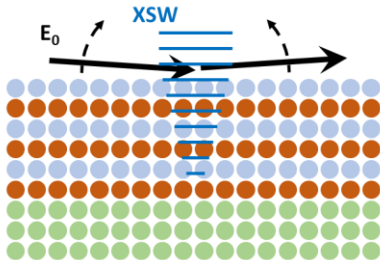
Grazing Emission - XRF



Total reflection - XRF



Depth profiling  
measurements



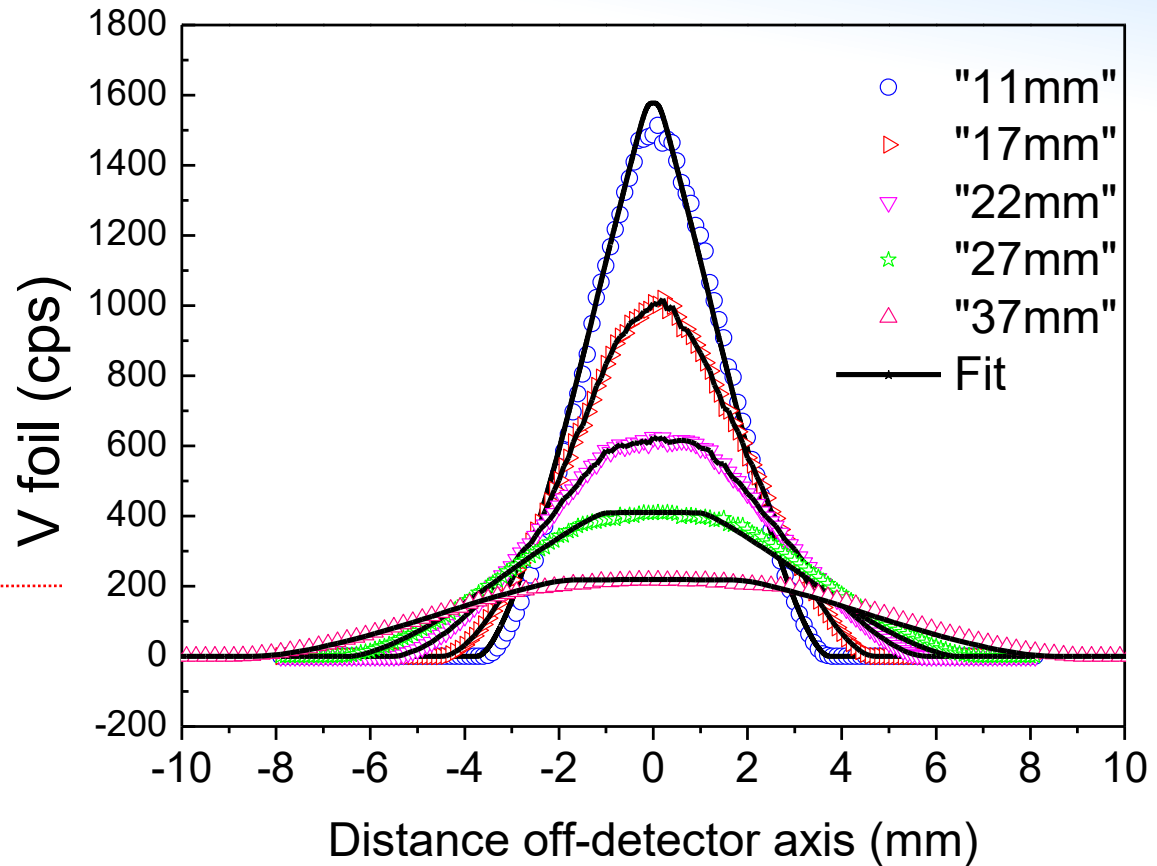
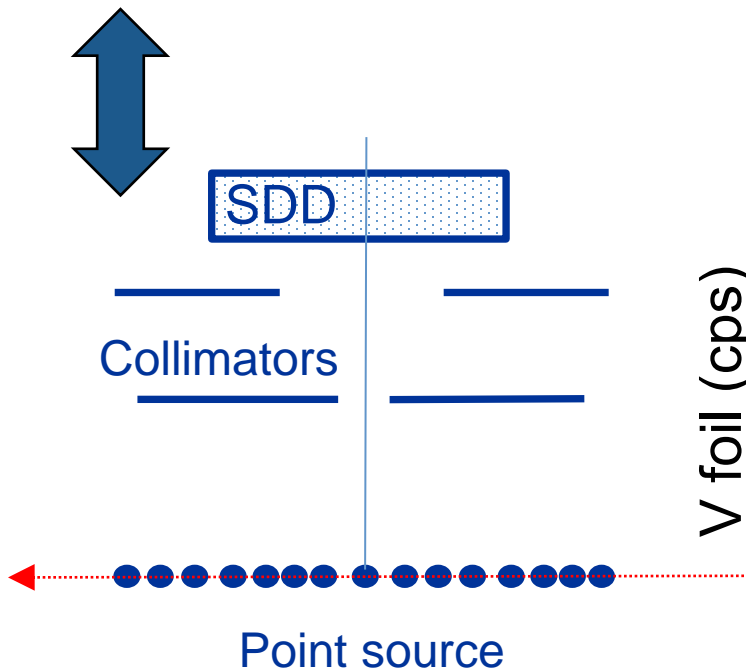
X-Ray Reflectometry

Trace element analysis  
Surface contamination



X-ray Absorption Spectroscopy  
(in TXRF geometry)

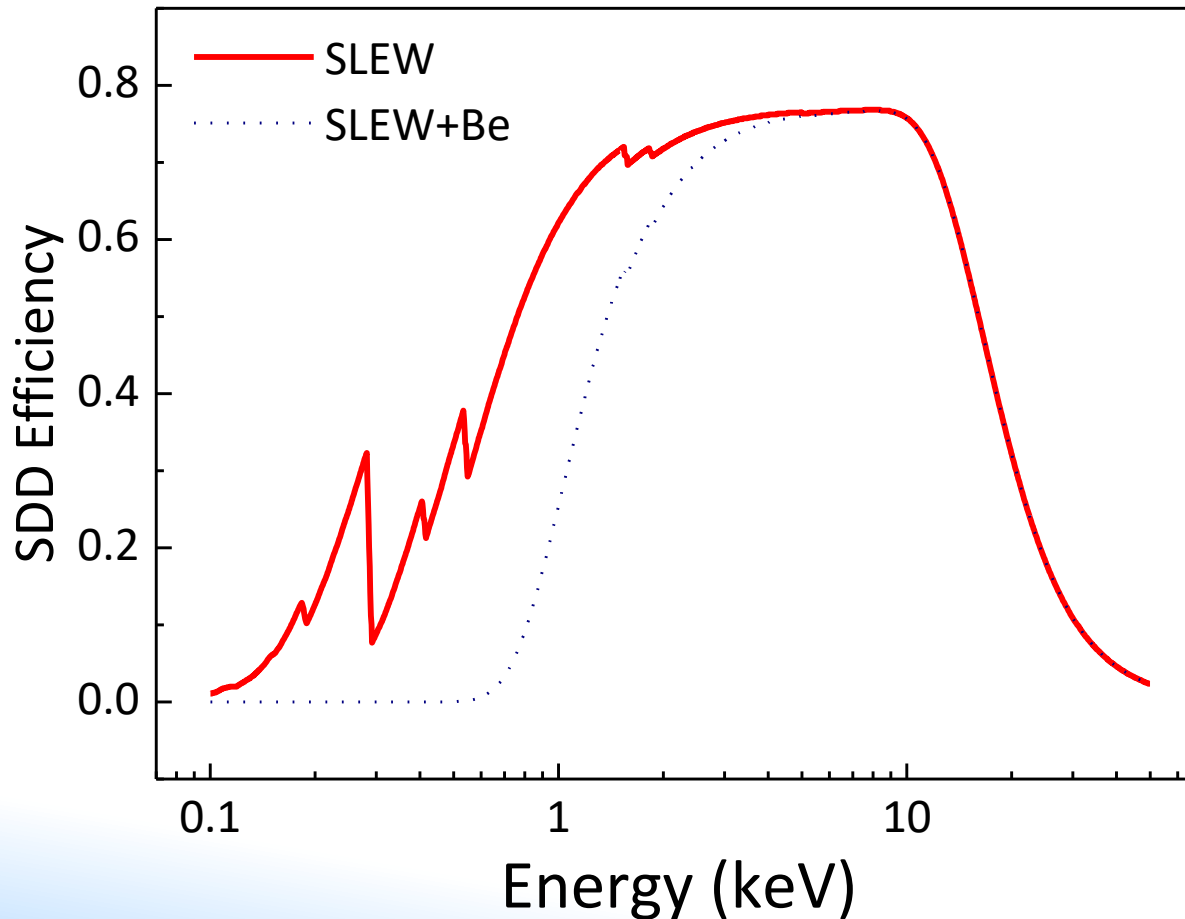
# □ GIXRF Geometry aspects



2.25 mm and 4.7 mm collimators

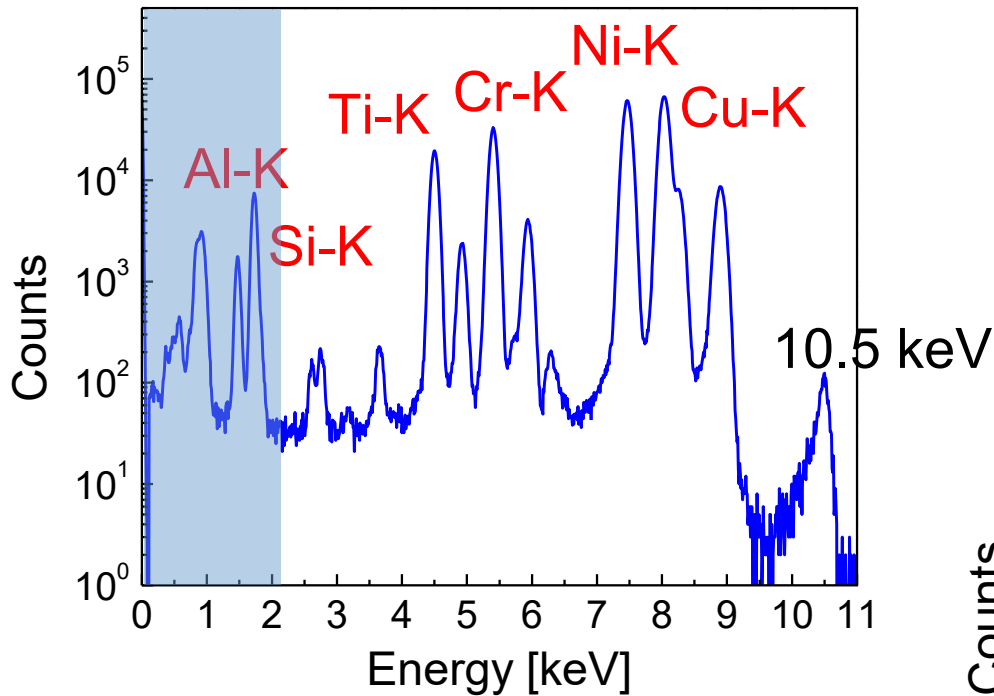
# □ SDD analysis modes (UTW/Be+UTW)

X-ray detector efficiency

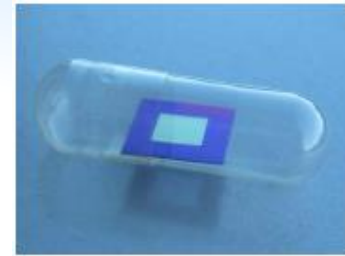


# Elemental XRF sensitivities

10 mins measurement, 2.4 GeV mode

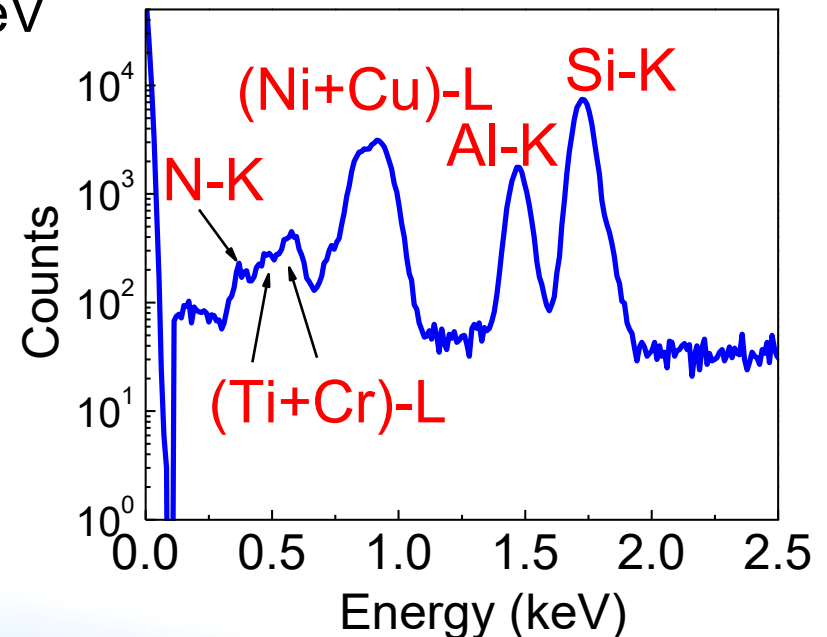


Beam dimensions @ 10.5 keV  
260 μm (H) 110 μm (V)



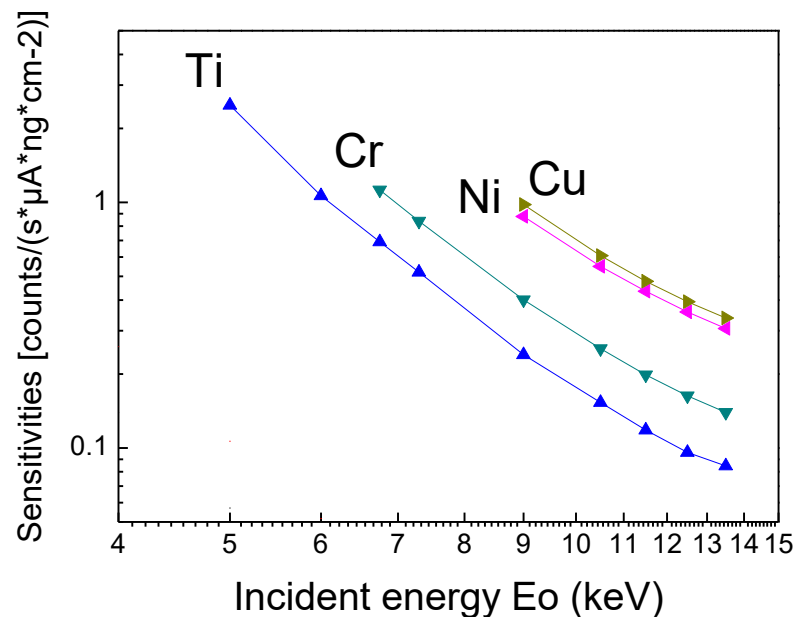
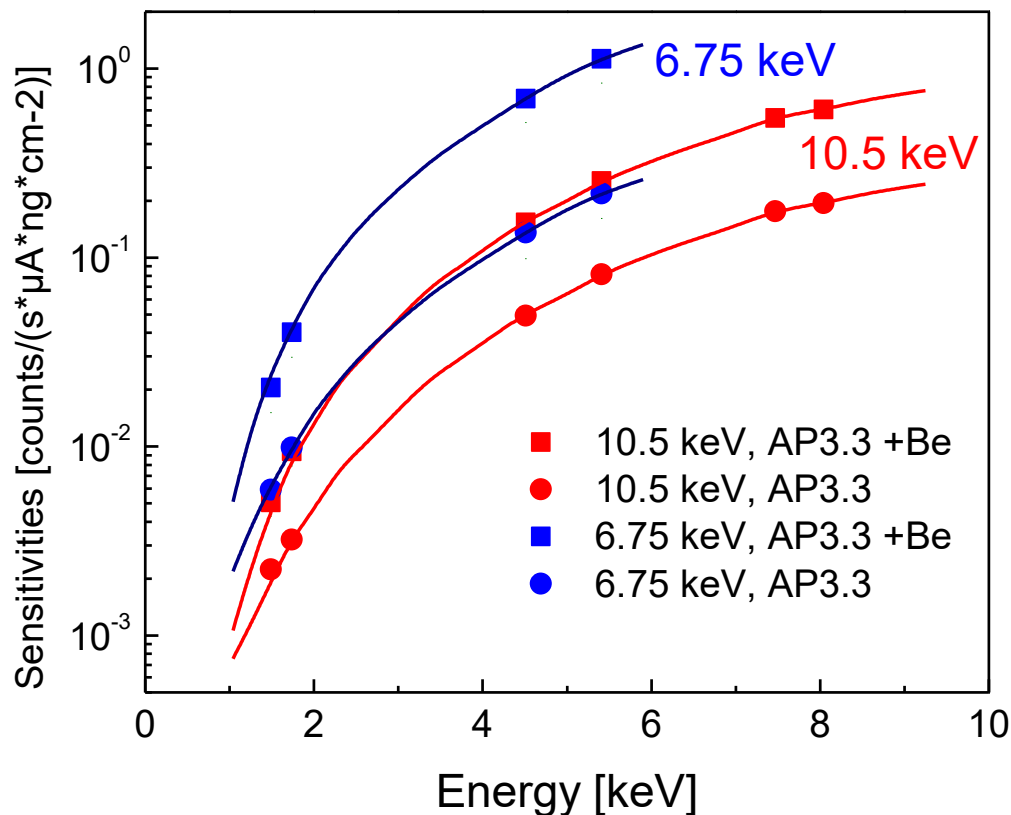
AXO Dresden

Cr/Al/Ni/Cu/Ti/ Si<sub>3</sub>N<sub>4</sub> 200 nm,  
each layer about 10 μg/cm<sup>2</sup>



# Elemental sensitivities, Exp. vs MC

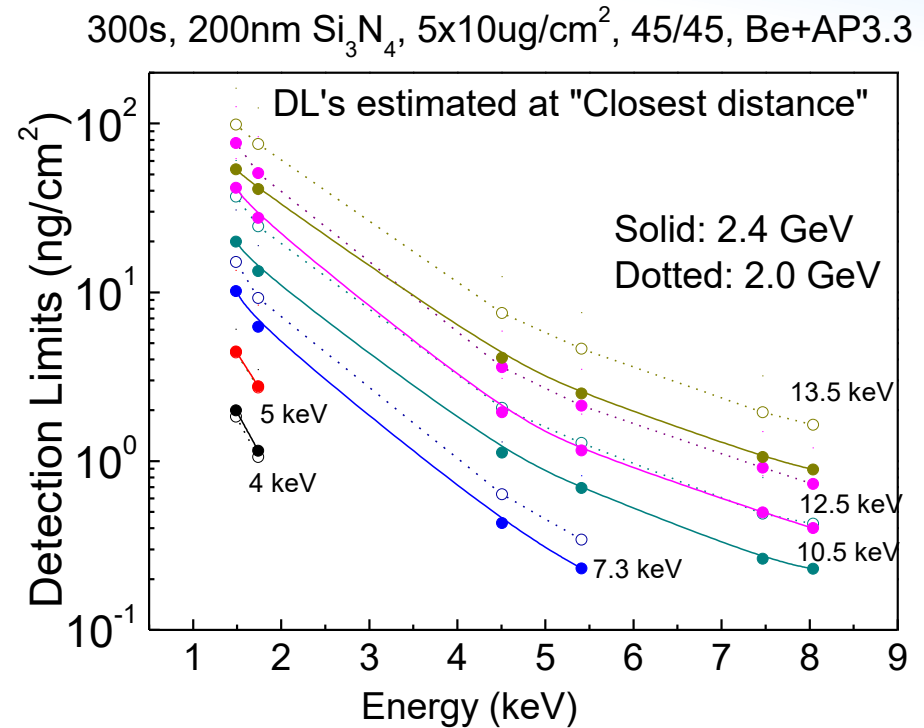
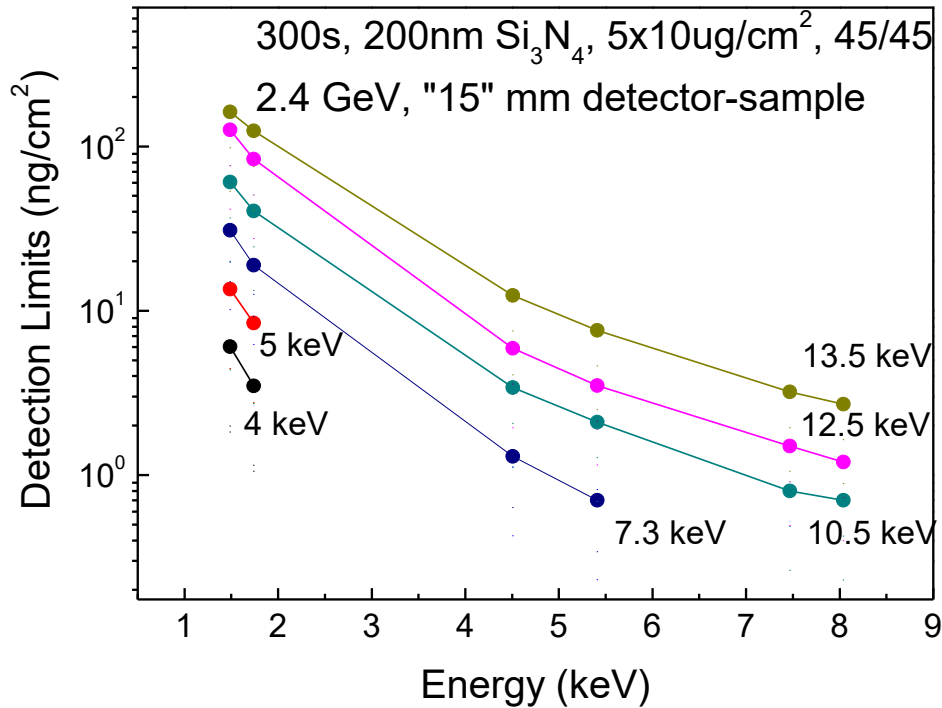
Experimental Sensitivities, XMI-MSIM MC calculations



**Sensitivities: counts/(s\*μA\*ng\*cm<sup>-2</sup>)**

# □ Detection limits from thin sample

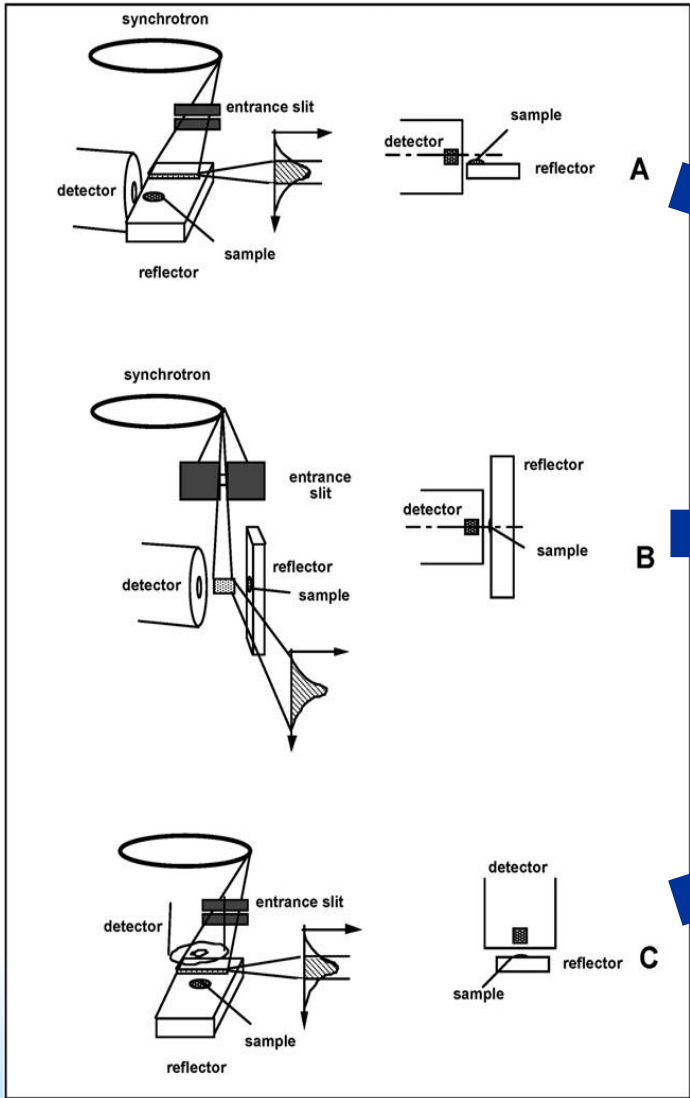
**Si<sub>3</sub>N<sub>4</sub> 200 nm membrane, with 10ug/cm<sup>2</sup> of Cr/Al/Ni/Cu/Ti**



**Detection limits (Al - Cu): 2 - 0.2 ng/cm<sup>2</sup>**

# □ Detector geometry for TXRF

The beam is naturally vertically collimated (0.1-0.2 mrad) and has linear polarization in the orbit plane



**Good excitation**  
**No scattering**  
**Poor detection**

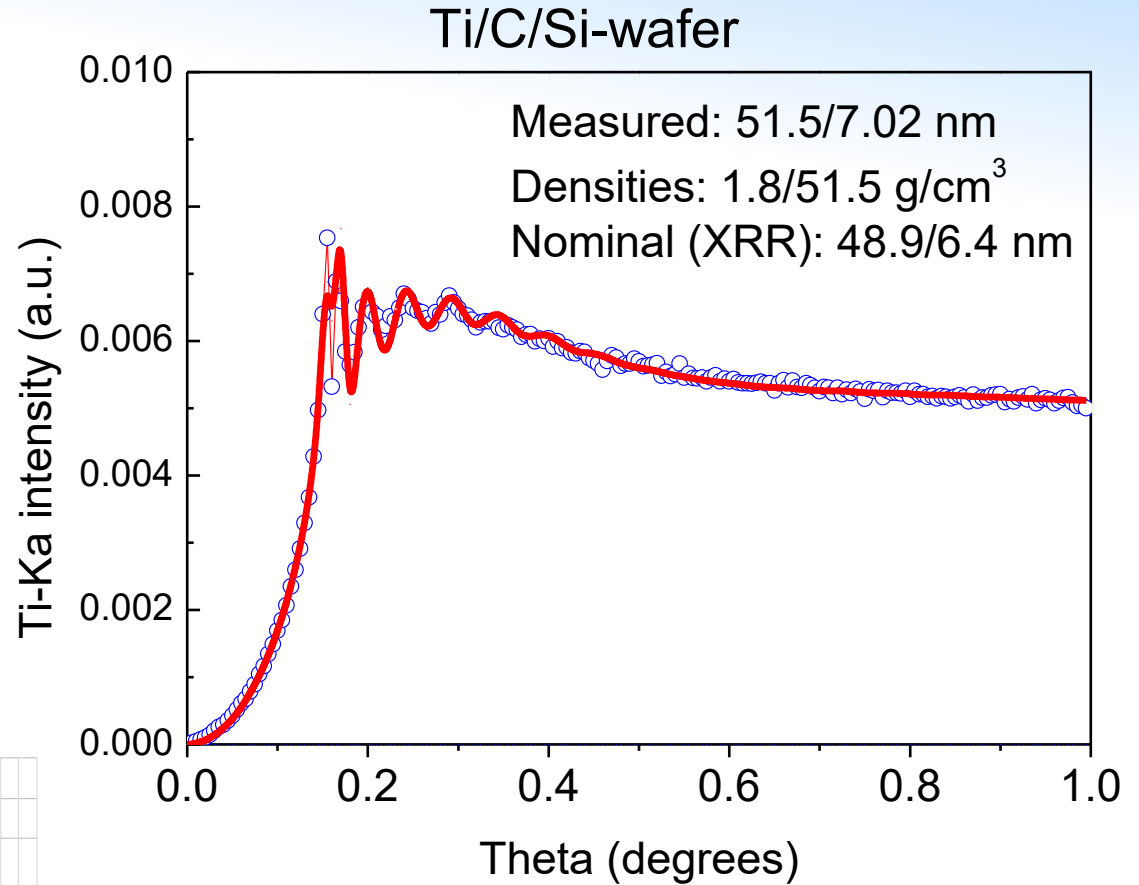
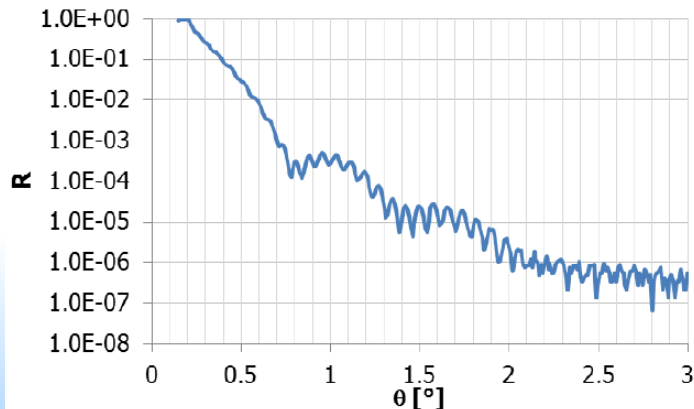
**Poor excitation**  
**No scattering**  
**Good detection**

**Good excitation**  
**Scattering**  
**Good detection**

C. Strel, P. Wobrauschek, F. Meirer and G. Pepponi,  
*Synchrotron radiation induced TXRF*, J. Anal. At. Spectrom.,  
 2008, 23, 792–798, DOI: 10.1039/b719508g

# □ GIXRF: C/Ti double layer

Prepared and characterized by AXO Dresden

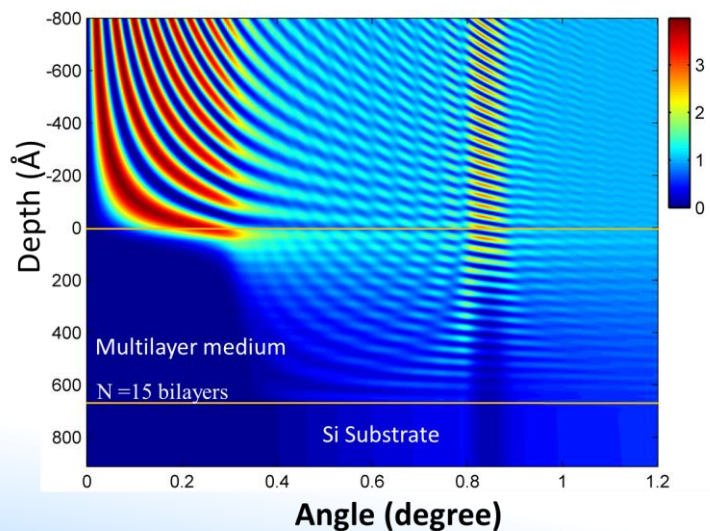
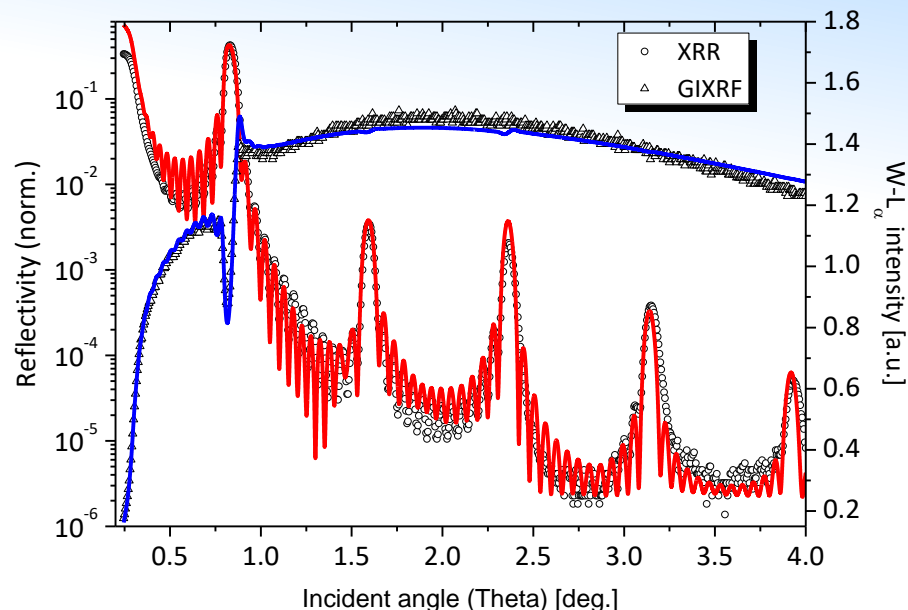
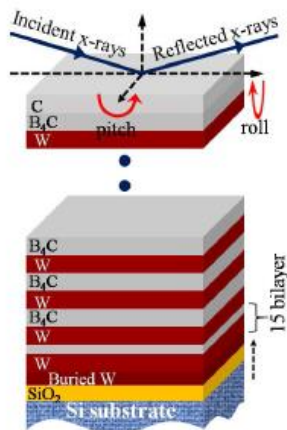


	Fit	Nominal
Ti (nm)	7.0	6.4
C (nm)	51.5	48.9



# W/B<sub>4</sub>C multilayered (x15) thin film

Multilayered sample, prepared by the Ramanna Center for Advanced Technology, Indore, India



Layer Material	Periodicity	'B <sub>4</sub> C'/'W' multilayer		
		Thickness (nm)	Roughness (nm)	Density (g/cm <sup>3</sup> )
B <sub>4</sub> C	14	1.9 ± 0.1	0.2 ± 0.1	2.10 ± 0.2
W		2.4 ± 0.2	0.3 ± 0.1	16.0 ± 0.2
B <sub>4</sub> C	1	2.1 ± 0.6	0.45 ± 0.2	2.3 ± 0.2
W		3.6 ± 0.3	0.55 ± 0.2	15.5 ± 1.0
SiO <sub>2</sub>	1	2.0 ± 0.3	0.5 ± 0.2	2.0 ± 0.3

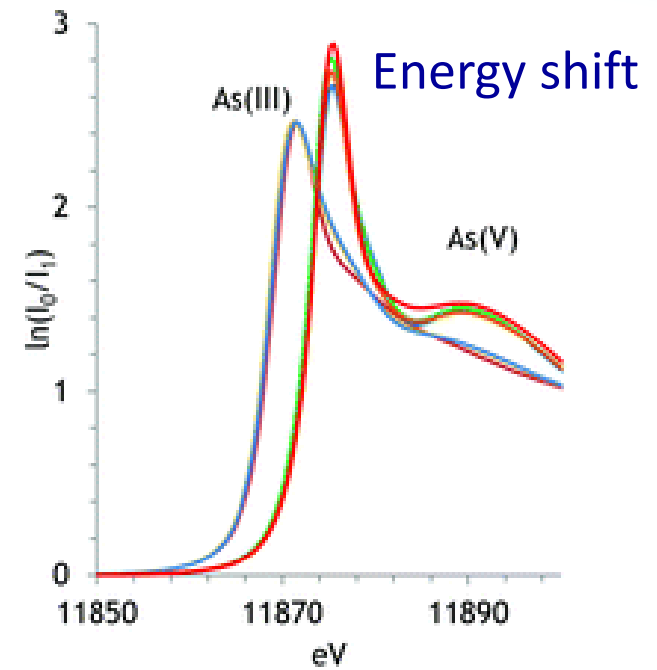
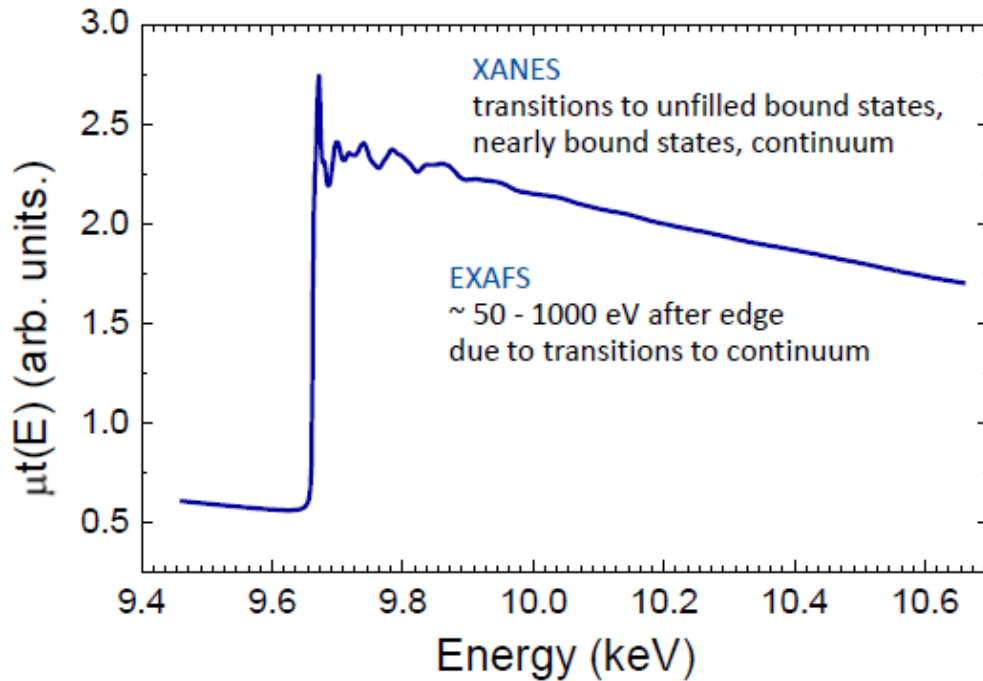
Electric Field Intensity (Normalized)

good agreement with previous analyses performed at the BL-16 beamline of Indus II

# X-ray Absorption Spectroscopy

XANES: local site symmetry, oxidation state, orbital occupancy

EXAFS: local structure (bond distance, number and type of neighbors)



Fine structure is affected by energy and density of electronic states and transition probabilities

Extended fine structure presents oscillated pattern due to constructive and destructive interferences of the outgoing photo-e wave with neighbor atoms.

# Zn speciation in fractionated APM

## 9-stage May-type cascade impactor

Sampling of size fractionated aerosol, down to 0.07 $\mu$ m size  
20-3200 L of air



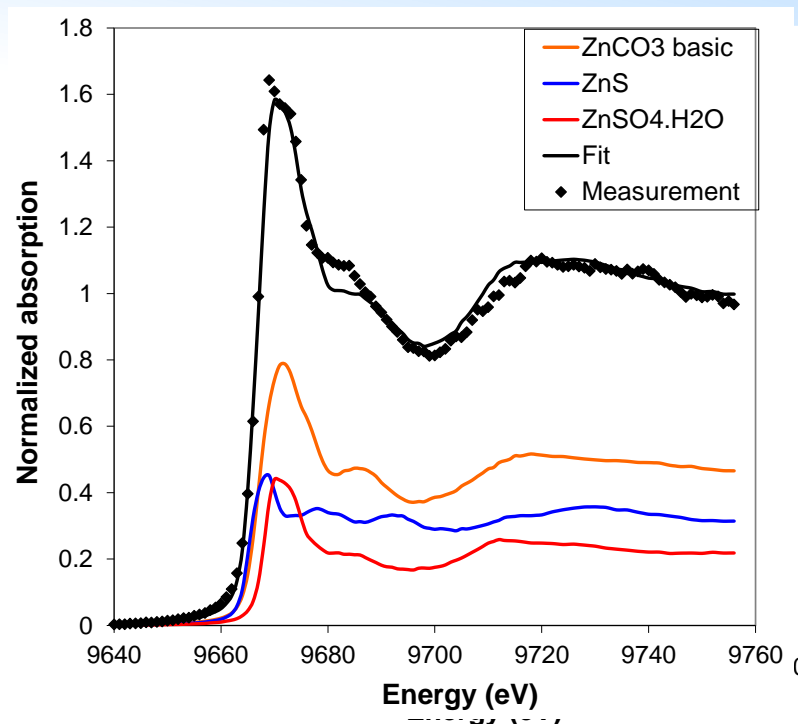
Deposited particles form a stripe of 200-500  $\mu$ m width on the 20x20 mm<sup>2</sup> Si wafer



## Sample geometry well suited to SR-TXRF-XANES investigations!

J. Osan, Environmental Physics Department,  
Centre for Energy Research, Budapest, Hungary

\*Self-absorption correction as described in: Osán J et al.,  
Spectrochim Acta Part B 65 (2010) 1008-1013



Sample: Paks (Hungary) 0.3-0.6  $\mu$ m, Zn content: 7.39 mg/m<sup>3</sup> (84 ng on 20 mm strip)

38% ZnSO<sub>4</sub>, 40% ZnS, 22% Zn in glass\*

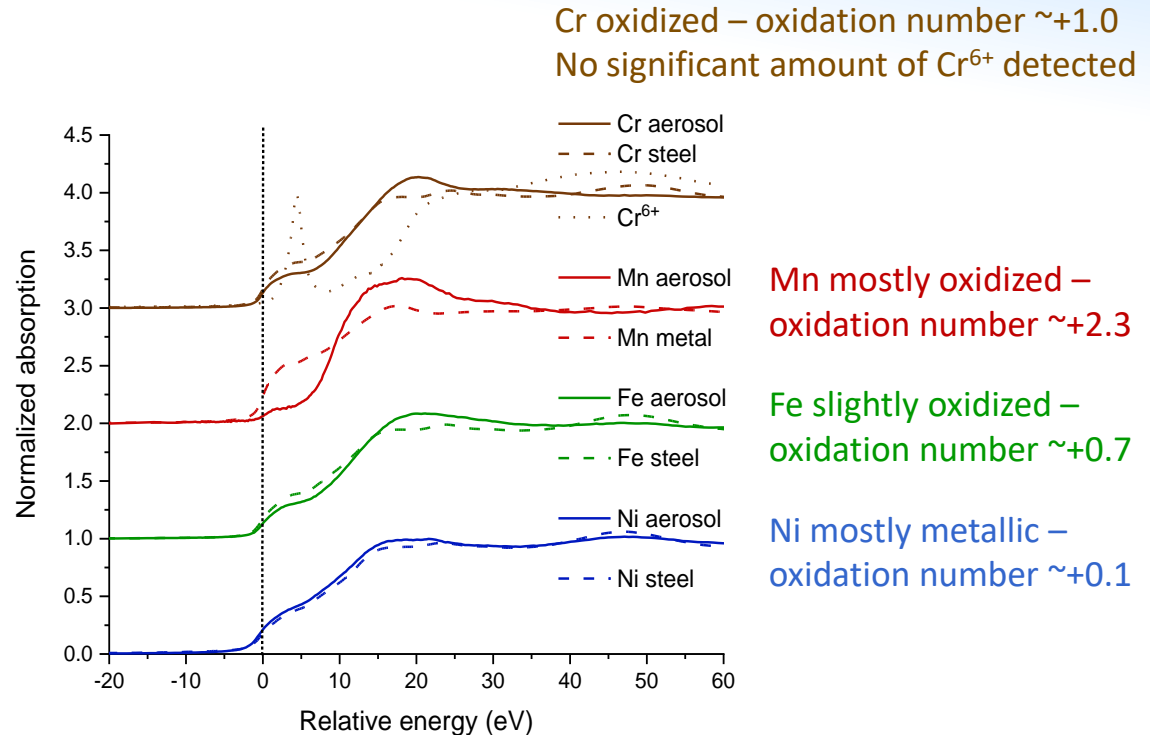
Main source: Iron smelter burning of painted wood

# Aerosols from 3D metal printing



Figure courtesy: Attila Nagy, Wigner FK, Budapest, Hungary

## XANES: Elettra XRF and XAFS beamlines



Most of emitted aerosol particles are in the ultrafine range

Oxidation number increases with decreasing particle diameter – important for estimation of health effects

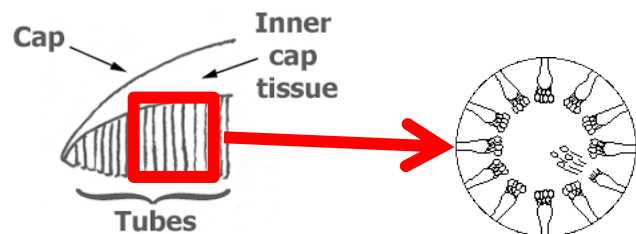
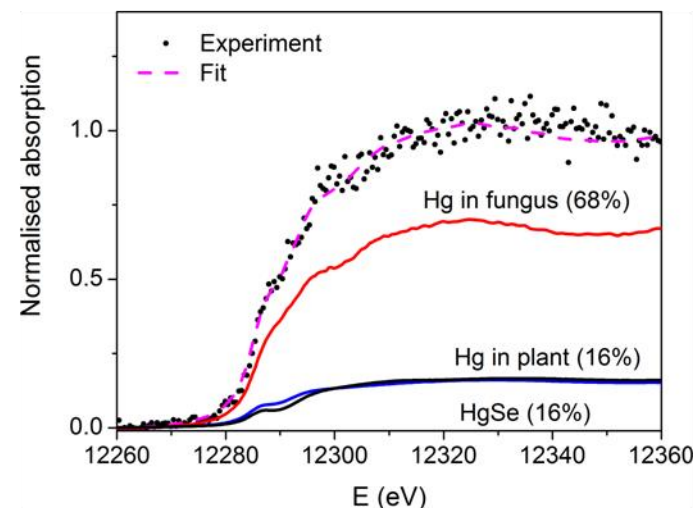
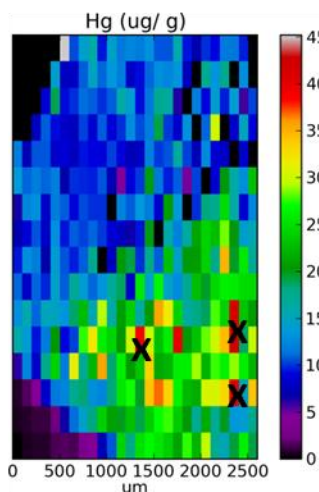
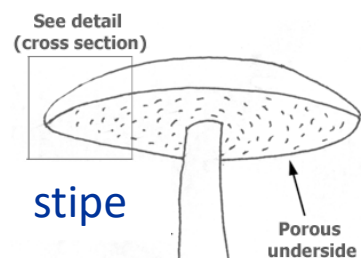
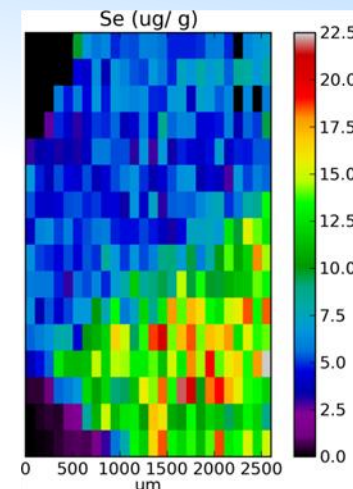
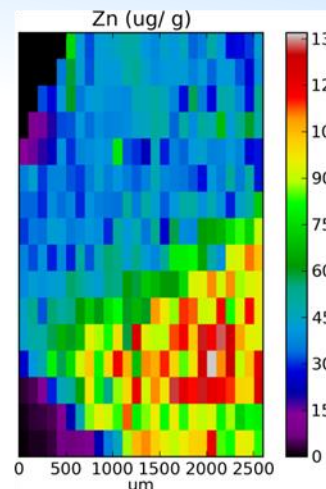
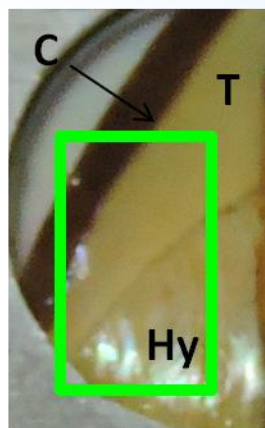
S. Kugler et al., Spectrochim. Acta Part B 2021, 177, 106110

# Se and Hg in edible mushrooms

K. Vogel-Mikuš<sup>1</sup>, P. Kump<sup>2</sup>, I. Arčon<sup>3</sup>

<sup>1</sup> Biotechnical faculty, University of Ljubljana, <sup>2</sup> Jozef Stefan Institute,

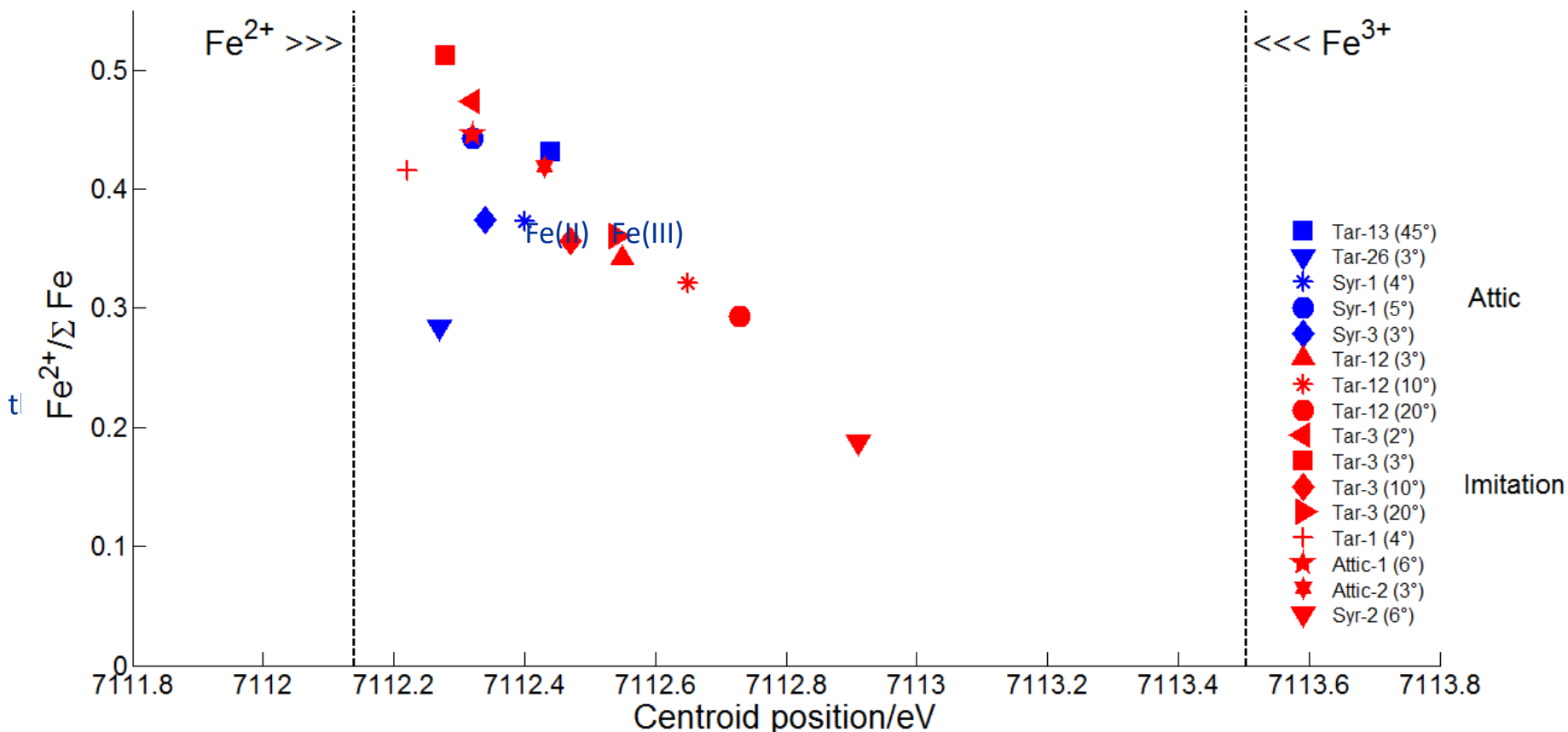
<sup>3</sup> University of Nova Gorica



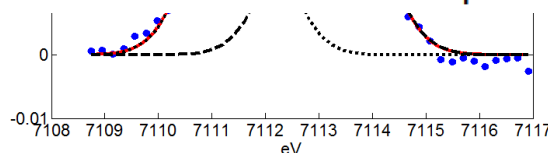
Hg is bound to tetra-cysteine proteins (metallothioneins). These proteins are digested by enzymes in the stomach and Hg is released and absorbed in our body.

# GI-XANES on Black Glaze

Fe-based decorations of Ancient ceramics manufactured in South Italy

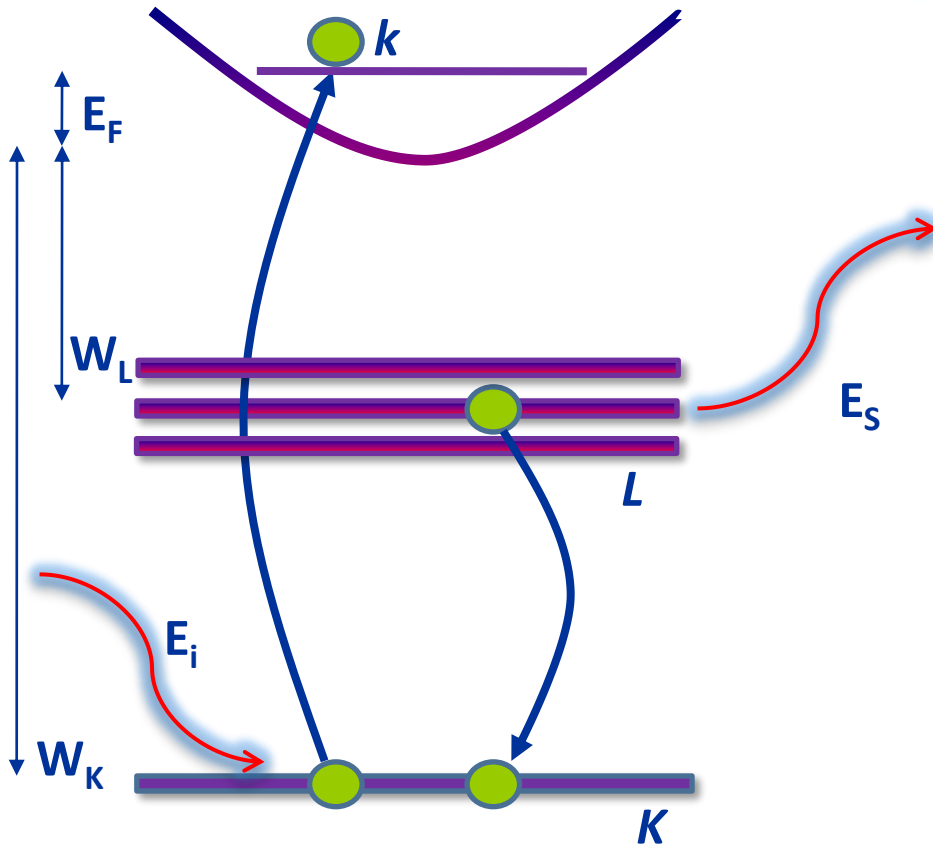


Taranto Archeological  
Museum Apulo f.r.  
Anonymous (Half IV  
cent. b.C.)



P. Romano, C. Caliri  
INFN-LNS, Catania, Italy

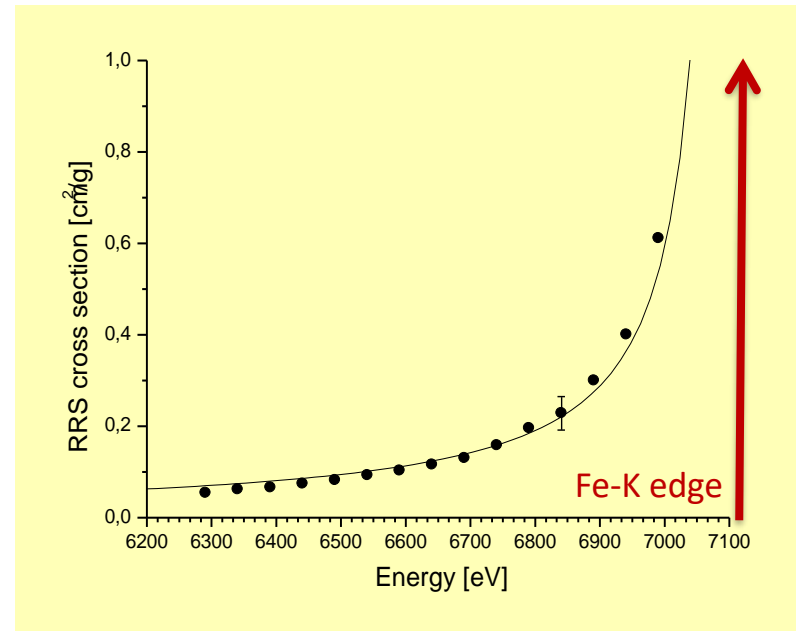
# Resonant inelastic X-ray scattering



$E_s$  = emitted photon energy  
 $E_i$  = incident photon energy  
 $\Omega_{K/L}$  = K/L binding energy  
 $E_F$  = Fermi energy  
 $k$  = photoelectron energy

$$E_s = E_i - \Omega_L - E_F - k$$

Courtesy of J.J. Leani, CONICET, Argentina



Measured KL-RIXS cross section for Fe (points) and a non-linear fitting to an expression with the functional form of the theoretical cross section (solid line)

# Elemental speciation in contaminated water by TR-RIXS

The toxicity and mobility of metal species varies with oxidation state and chemical environment

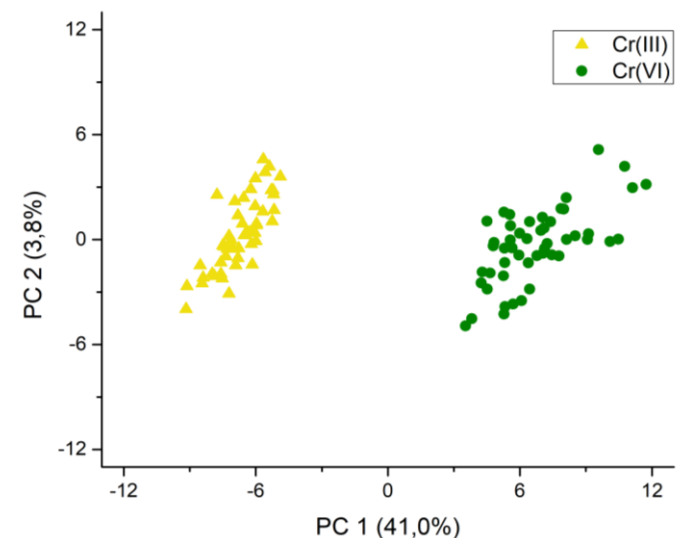
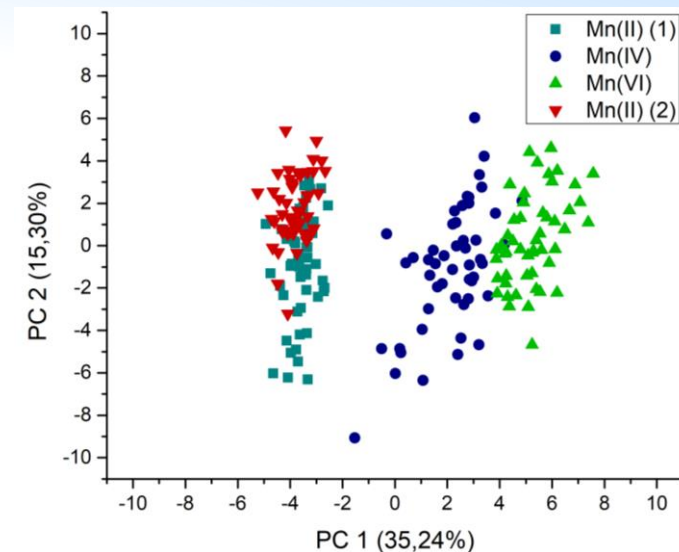
The analyzed samples consisted of droplets dried on silicon wafers. The solutions consisted of the different compounds diluted in distilled water (to 1 % by mass concentration).

- Two chromium compounds,  $\text{CrCl}_3$  (+III),  $\text{K}_2\text{CrO}_4$  (+VI),
- Four manganese species  $\text{MnCl}_2 \cdot (\text{H}_2\text{O})$  (+II),  $\text{KMnO}_4$  (+VI),  $\text{Mn}(\text{H}_2\text{PO}_2)_2$  (+II) and  $\text{MnO}_2$  (+IV) were studied.

Incident photons energy was set 10 eV below the K-edge binding energy, i.e. 6529 eV (Mn) and 5979 eV (Cr), under TXRF conditions.

50 spectra of each sample acquired (5 min each). A PCA procedure was performed over the selected energies (RIXS peaks).

J.I. Robledo *et al.*, *Anal. Chem.* **90**, 3886 (2018)





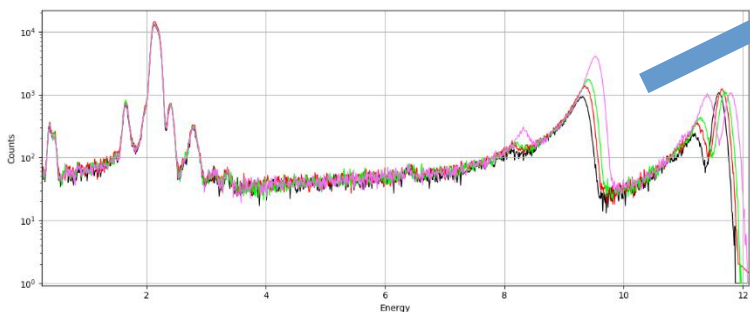
# Analysis of gold samples

## Absorption edges of Pt and Au

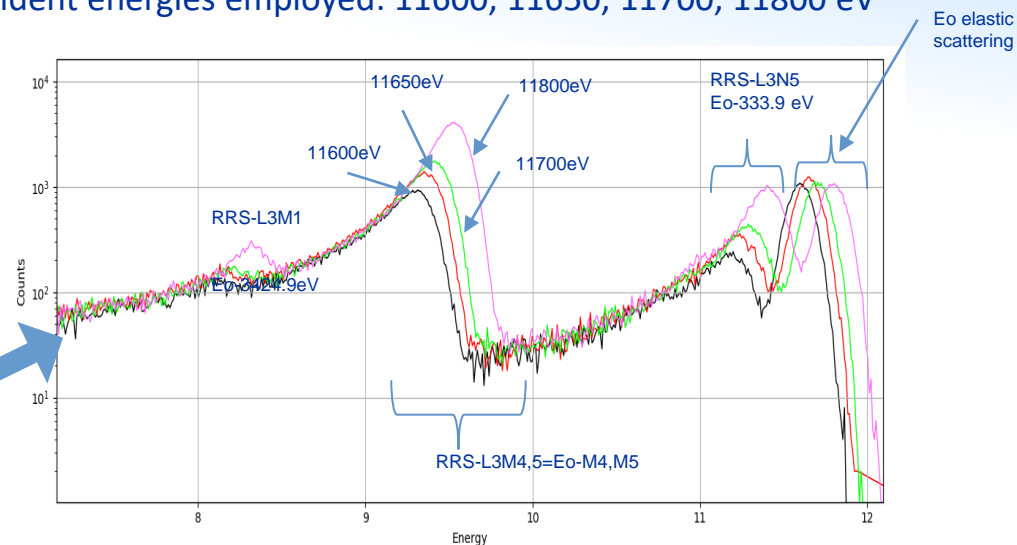
	Pt	Au
Z	78	79
L1 (keV)	13.88	14.353
L2 (keV)	13.273	13.734
L3 (keV)	11.564	11.919

Pt La: 9.44 keV

## Synchrotron XRF spectra of pure (99.99%) thick (thickness 25 $\mu\text{m}$ ) gold samples



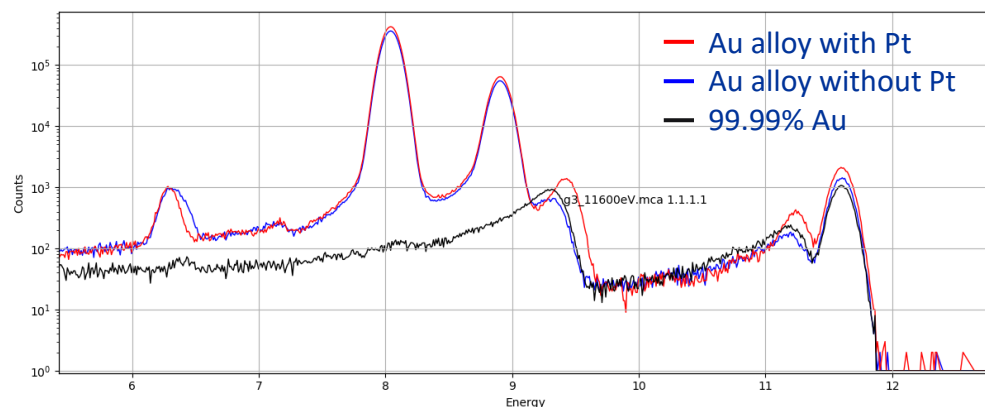
Incident energies employed: 11600, 11650, 11700, 11800 eV



## Eo=11600 eV @Elettra

Pure gold spectrum vs. Gold alloy with 0.15% Pt (Au:65.56%, Cu:25.21%, Ag:9.08%) and vs. a different certified alloy of similar composition without Pt

11600 eV > Pt(U\_L3)=11564 eV



Courtesy of A.G.Karydas, (National Center for Scientific Research "Demokritos", Greece)

School on Synchrotron Light Sources and their Applications, 15-26 January 2024



**IAEA**

International Atomic Energy Agency

***Thanks for your attention!***

Alessandro Migliori

[a.migliori@iaea.org](mailto:a.migliori@iaea.org)

<https://nucleus-new.iaea.org/sites/nuclear-instrumentation/Pages/Home.aspx>

<https://www.elettra.trieste.it/lightsources/elettra/elettra-beamlines/microfluorescence/x-ray-fluorescence.html>